Paleo-oxygenation and Uranium Isotope Behavior in Lower Mississippian Black Shales of North America

A Thesis submitted in partial fulfillment of the requirements for the degree of Master of Science at George Mason University

by

Randolph L Rutledge
Bachelor of Science
George Mason University, 2022

Director: Geoffrey Gilleaudeau, Assistant Professor
Department of Atmospheric, Oceanic, and Earth Science

Fall 2022
George Mason University
Fairfax, VA

DEDICATION

I dedicate this work to my mom Dawn Rutledge and my grandfather James T Rutledge Sr.

ACKNOWLEDGEMENTS

I wish to thank my advisor, Dr. Geoffrey Gilleaudeau, for his guidance and support throughout this process. I also want to thank the members of my committee for their invaluable input and infinite patience: Dr. Linda Hinnov, Dr. Thomas Algeo, and Dr. Randolph McBride. Finally, my work would not have been possible without generous grants from the Geological Society of America, American Association of Petroleum Geologists, and the Society for Sedimentary Geology.

TABLE OF CONTENTS

LIST OF TABLES

LIST OF FIGURES

ABSTRACT

PALEO-OXYGENATION AND URANIUM ISOTOPE BEHAVIOR IN LOWER MISSISSIPPIAN BLACK SHALES OF NORTH AMERICA

Randolph L Rutledge, M.S.

George Mason University, 2022

Thesis Director: Dr. Geoffrey Gilleaudeau

Uranium isotopes in ancient sedimentary rocks have emerged as a powerful proxy for the oxygenation history of Earth surface environments. Proper quantitative interpretation of uranium isotope data hinges, however, on an understanding of isotope fractionation associated with uranium removal to sediments under different redox conditions. Whereas oxygenated environments are plentiful in the modern ocean, studying contemporaneous uranium isotope behavior under a range of low-oxygen conditions is difficult given the paucity modern anoxic basins. For example, it is not possible to simultaneously test uranium isotope fractionation under oxic, euxinic, and ferruginous marine conditions using modern analogues. Here, we present uranium isotope data from coeval Lower Mississippian shales of the Appalachian Basin (North America) that represent a range of redox conditions. Iron speciation and trace metal data indicate that the Tournaisian Sunbury Shale was deposited across a strong redox gradient, from oxic to

equivocal conditions proximal to the Catskill Delta in the northeast, to ferruginous conditions in the basin trough, to euxinic conditions towards the basin-bounding Cumberland Sill in the southwest. Overall, we find that both euxinic and ferruginous environments are capable of imparting high degrees of U isotope fractionation, and that U isotope values correlate more strongly with total organic carbon (TOC) and trace metal proxies for productivity than they do with euxinic vs. ferruginous conditions. We also compared our data to coeval carbonates from Nevada, which can be used to estimate Early Mississippian seawater U isotopes values. We find that cores deposited under more stably anoxic conditions below the redoxcline and under consistently brackish salinities away from direct freshwater sources record an increasing U isotope value through time, which loosely mirrors global seawater values. By contrast, cores deposited close to the Catskill Delta and in a shallow mixing zone near the Cumberland Sill show a decreasing U isotope trend through time which is the opposite of global seawater, indicating entirely local controls on U isotope fractionation. Ultimately, these results suggest that highly productive environments with high organic carbon loading can exert a strong control on the global U isotope mass balance regardless of whether euxinic or ferruginous conditions are present. These results necessitate a partial reassessment of the processes controlling seawater U isotope variability through Earth history.

INTRODUCTION

Uranium isotope analysis has become a powerful tool for understanding redox conditions in ancient water bodies, with particular focus on the relationship between ocean oxygenation and biological evolution through Earth history. This analytical method has been used previously to understand global ocean redox conditions across a wide range of geologic time, with some recent examples including analysis of mudrock samples spanning from the late Neoproterozoic to the middle Paleozoic (Lu et al., 2020), analysis of carbonate rocks to estimate the level of seafloor euxinia during the mid-Proterozoic (Gilleaudeau et al., 2019), and carbonate analysis to constrain changing redox conditions of the global oceans during glacial retreat following the Sturtian Snowball Earth (Lau et al., 2017). Much work has also focused on understanding the link between global anoxia and Phanerozoic mass extinction events (e.g., Brennecka et al., 2011). Uranium isotope fractionation is also tied to biotic reduction, giving uranium isotopes the ability to uniquely fingerprint microbial activity in ancient water bodies (Stylo et al., 2015).

Advances in mass spectrometry over the past decade have allowed for the detection of minute mass differences to precisely determine isotope ratios of very heavy chemical elements such as uranium. Uranium is dominated by two long-lived isotopes, ^{238}U and ^{235}U. ^{238}U has a half-life of 4.468 Gyr while ^{235}U has a half-life of 700 Myr. Uranium exists in two redox states in water bodies based on the availability of oxygen and presence/absence

of a variety of reductants. In the presence of oxygen, soluble uranium exists as U(VI). Uranium in an anoxic setting is reduced from U(VI) to U(IV), and this insoluble U(IV) is removed from the water into sediment and can be preserved in anoxic mudrocks. The heavier uranium isotope, ^{238}U, is preferentially removed under anoxic conditions, concentrating ^{238}U in anoxic sediments and leaving residual water bodies with an abundance of ^{235}U.

Uranium has a residence time of 400 kyr in the modern oceans, which is substantially longer than the ocean mixing time. The mean $\delta^{238}U$ value of modern seawater is $-0.39 \pm 0.01‰$ and U is well-mixed across the oceans with a uniform open ocean concentration of ~3.2 ng/g (Tissot and Dauphas, 2015). There are a number of sinks for U in the modern oceans, including ferromanganese oxide sediments, hydrothermally-altered basalt, carbonate sediments, suboxic sediments, and anoxic sediments (Cole et al., 2020). Anoxic sediments are thought to impart the largest degree of isotopic fractionation, thus making uranium isotope fractionation a powerful proxy for the extent of anoxia in modern and ancient oceans.

The utility of U isotopes as a paleo-redox proxy depends, however, on our understanding of U removal and isotopic fractionation under different redox conditions. For most previous studies that model paleo-ocean redox using U isotopes, a large fractionation factor between seawater and sediments is assumed for all anoxic environments (e.g., Zhang et al., 2018). Removal of isotopically heavy U to anoxic sediments leaves the oceans enriched in light U isotopes; thus, shifts towards light U isotopes in the ancient carbonate record are commonly interpreted as expansions of marine

anoxia. This interpretation is based, however, on data largely from modern euxinic (anoxic + sulfidic) settings such as the Black Sea (Montoya-Pino et al., 2010; Andersen et al., 2014; Rolison et al., 2017), Saanich Inlet (Holmden et al., 2015), Cariaco Basin (Andersen et al., 2014), and Framvaren Fjord (Kaltenbach, 2012). In euxinic settings, fractionation factors between sediments and seawater are between +0.4 and +1.2‰. Laboratory biologically-mediated U reduction experiments have also shown large fractionation factors during U reduction that matches fractionation factors observed during reduction in modern euxinic settings.

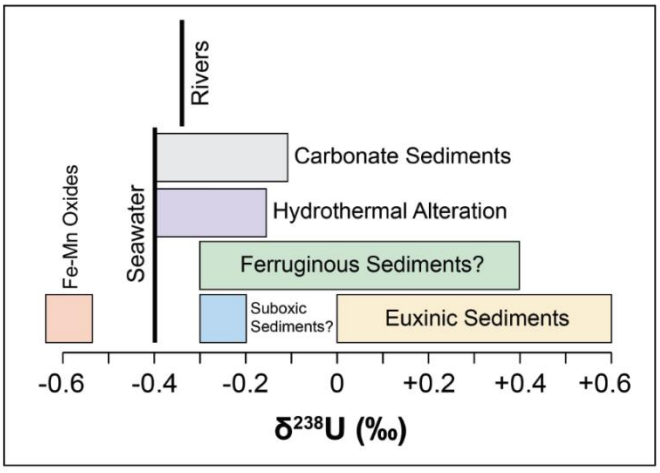

Figure 1. Uranium isotope composition of rivers, seawater, and various oceanic sinks.

However, many anoxic settings in the ancient oceans may have been non-euxinic and had other primary redox buffers such as dissolved Fe(II) (i.e., ferruginous conditions) (Poulton and Canfield, 2011). It is critical to understand U isotope fractionation under anoxic, non-sulfidic conditions so that we can understand how to interpret U isotope data during periods of widespread ferruginous oceans. This is difficult, however, because of a lack of modern analogues; there are no ferruginous environments in the modern oceans due to the high sulfate concentrations of modern seawater. While there are no open ocean ferruginous waters available on Earth today, there are some lakes that can be investigated. Brownie Lake in Minneapolis, MN, USA is a permanently stratified body of water with anoxic conditions below a shallow pycnocline, a high concentration of dissolved iron in anoxic waters, and low levels of sulfate. This makes it a promising analogue for ancient seas with ferruginous conditions. Cole et al., (2020) analyzed uranium isotope compositions in two sediment cores from Brownie Lake spanning both oxic and ferruginous environments. $\delta^{238}U$ values from the lower anoxic core had a mean of $-0.07 \pm 0.59‰$, whereas the higher oxic core had a mean of $-0.15 \pm 0.18‰$. Although $\delta^{238}U$ values in the anoxic core do show higher variability than those in the oxic core, Cole et al. (2020) concluded that sediment $\delta^{238}U$ values were similar in both oxic and ferruginous settings, challenging the notion that all anoxic environments lead to large U isotope fractionations. This potentially complicates the interpretation of ancient U isotope data, suggesting that a ferruginous ocean would look similar to an oxic ocean in terms of U isotopes (Cole et al., 2020). Gilleaudeau et al. (in prep) also investigated ferruginous Canyon Lake, Michigan, USA and found a similar lack of U isotope fractionation under ferruginous conditions.

In addition, laboratory experiments found that U reduction in the presence of Fe(II) actually drove U isotope fractionation in the opposite direction, pulling light isotopes out of solution, leaving the solution enriched in heavy isotopes (Stylo et al., 2015). This study concluded that specific biological enzymatic pathways were the main determinant of U isotope fractionation during U reduction. Due to these uncertainties, it is clearly critical that we investigate coeval oxic, euxinic, and ferruginous environments in order to understand how U isotopes are fractionated differently under different redox conditions. This is necessary to properly interpret U isotope data from ancient oceans that may have been characterized by a wide variety of redox conditions.

Here, we investigate U isotopes across a redox gradient in the Lower Mississippian Sunbury Shale, Appalachian Basin, USA. The Devonian-Mississippian saw major shifts in the landscape of Earth, with a large increase in biologically-mediated bedrock weathering as rooted plants and trees created substantial soil development for the first time in Earth history. North America developed a series of epicontinental seas during this period, and an increased flux of nutrients into these waterways caused widespread anoxia (Algeo and Scheckler, 1998). Devonian-Mississippian black shale found across North America records this period of widespread anoxia and increased preservation of organic material in epicontinental seas.

Gilleaudeau et al. (2021) performed a watermass reconstruction study across a lateral gradient through the Sunbury Shale in Ohio and Kentucky using both redox (iron speciation, trace metals, pyrite sulfur isotopes) and paleosalinity proxies (Sr/Ba) for the Early Mississippian Appalachian Seaway. This study found a strong redox gradient

between oxic conditions in the NE close to the Catskill Delta, ferruginous conditions in the basin trough in central Ohio, and euxinic conditions in the SW (Kentucky) close to the basin-bounding Cumberland Sill. We therefore measure U isotopes across this same redox gradient in order to understand U isotope fractionation in coeval marine oxic, ferruginous, and euxinic environments. This study is the first to investigate U isotope fractionation under coeval marine oxic, ferruginous, and euxinic redox environments, thus providing critical new information that will inform all future U isotope paleo-redox studies.

GEOLOGICAL BACKGROUND

Modern anoxia and its drivers

Modern anoxic environments occur where eutrophication takes place. This process occurs when excess nutrients like nitrogen and phosphorus are loaded to a body of water, causing a bloom of photosynthetic organisms. As this organic carbon rains down, there is a respiratory demand for oxygen at depth. Anoxic conditions result as respiration demands for O_2 outweigh ventilation (Adelson et al., 2001). Natural Oxygen Minimum Zones (OMZs) also occur when upwelling brings nutrient-rich deep water to the surface. Large mid-depth regions of anoxia and hypoxia settle at the continental margin typically between 200 and 1,500 m in depth (Helly and Levin, 2004). Oxygen levels decrease rapidly below the surface to the OMZ, then increase again below the OMZ as water mixes and respiration demands are lower. Anthropogenic nutrient delivery in modern systems increases the size and extent of anoxia in the water column. This human-induced eutrophication may be analogous to times in the geologic past when ocean anoxia expanded as a result of enhanced nutrient delivery from continental runoff. Devonian environments could be an example of this phenomenon, as the evolution of soils and land plants changed ocean chemistry (Algeo and Scheckler, 1998). Large igneous provinces and resulting increased continental weathering of fresh igneous rock are another example of a large-scale ocean chemistry change that could lead to an increase of global ocean anoxia. Such a scenario has been recorded across the Permo-Triassic extinction and across several Mesozoic ocean anoxic events (Wignall and Twitchett, 1996; Jenkyns, 2010).

The Gulf of Mexico 'Dead Zone' is a prolific expanse of anthropogenically-induced anoxia. It occurs annually between 50 and 150 km from the coast of Louisiana and reaches its greatest extent in the summer months (Rabalais and Turner, 2019). Phytoplankton growth in the late spring, followed by increased nutrient loading in the summer growing months contribute to widespread hypoxia. Hypoxia in the water column occurs between 5 and 60 m depth. The low oxygen layer is typically around 10 m thick (Bianchi et al., 2010). There are three distinct zones of hypoxia that are controlled by different processes. Closer to river mouths, phytoplankton blooms are reduced because water turbidity decreases sunlight. However, high levels of organic carbon in sediment allow for biotic reduction at the sediment-water interface. Further away from river mouths, water turbidity decreases, and phytoplankton blooms produce raining organic carbon in the water column, while nutrient load decreases. At the furthest reaches of the OMZ from the shore, nutrient load is minimal, but stratification in the water column allows for hypoxic conditions. Wind is another important factor in the formation of the Dead Zone. Eastward winds that occur during the autumn and winter months mix waters, which reoxygenates them. As these winds diminish during the spring and summer months, hypoxia emerges.

The Chesapeake Bay is another region where human activity causes anoxia. Data from as far back as 1917 show the presence of oxygen-depleted water below 10 m depth in the central basin (Adelson et al., 2001). Elevated levels of H_2S have been known to destroy marine organisms. Adelson et al. (2001) used molybdenum (Mo) geochemistry to track seasonal anoxia in the Chesapeake Bay. They found that after 1960, elevated levels of Mo, indicating an anoxic environment, were found variably in the sediment record. In

some years, anoxia is consistent for several months during the summer, but in others it never forms. Anoxia tends to form earlier in the year, and last longer in the northern section of the basin axis. Like in the Gulf of Mexico, the Chesapeake Bay Dead Zone's anoxic conditions are seasonal, driven by human activity, and vary based on hydrography of the basin.

Large scale open ocean OMZs have been increasing in size since the mid-20th century (Stramma et al., 2012). The expansion of anoxic and hypoxic conditions into more shallow waters disrupts marine ecosystems, and especially complex marine organisms dependent on high levels of dissolved oxygen. Many pelagic fish and other oxygen dependent species require around 3.5 ml l^{-1} dissolved oxygen levels or higher to sustain life. Historical dissolved oxygen data taken from HydroBase-2 in the eastern tropical Atlantic OMZ shows a decrease of around −0.01 ml l^{-1} yr^{-1} from 1960 to 2010. Forty-seven blue marlins were tagged and their vertical and horizontal movement in the OMZ was tracked. In areas where the available dissolved oxygen was above 3.5 ml l^{-1}, marlin went as deep as 200 m, while only diving 100 m in the OMZ. In order to understand the causes of anoxia in the geologic past, analogues from the present should be considered. Modern anthropogenic loading of excess nutrients to marine environments is relevant to the Devonian-Mississippian transition when enhanced terrestrial weathering and nutrient delivery related to land plant expansion caused widespread eutrophication and anoxic expansion in epicontinental seas across the globe.

Rabalais et al. (2014) investigated C, N, and S abundances and isotopes in seven cores from the Mississippi Bight in the Gulf of Mexico (Fig. 2). Concentrations of these

elements increased in the core above 50 cm depth, correlating to around 1940. The increase in carbon is linked to the abundance of photosynthetic organisms in the water column and higher preservation under anoxic conditions. Increases in N are due to the influx of nutrients from river sources and an increase in nitrogen fixation, as well as increased denitrification within the expanding OMZ. S increases and a shift towards lighter S isotopes are related to an increase in microbial sulfate reduction as oxygen depletion increased. The presence of H_2S in bottom-waters has been confirmed by divers. Lastly, the Mo flux to sediments has also increased associated with increased anoxic water volume (Fig. 2).

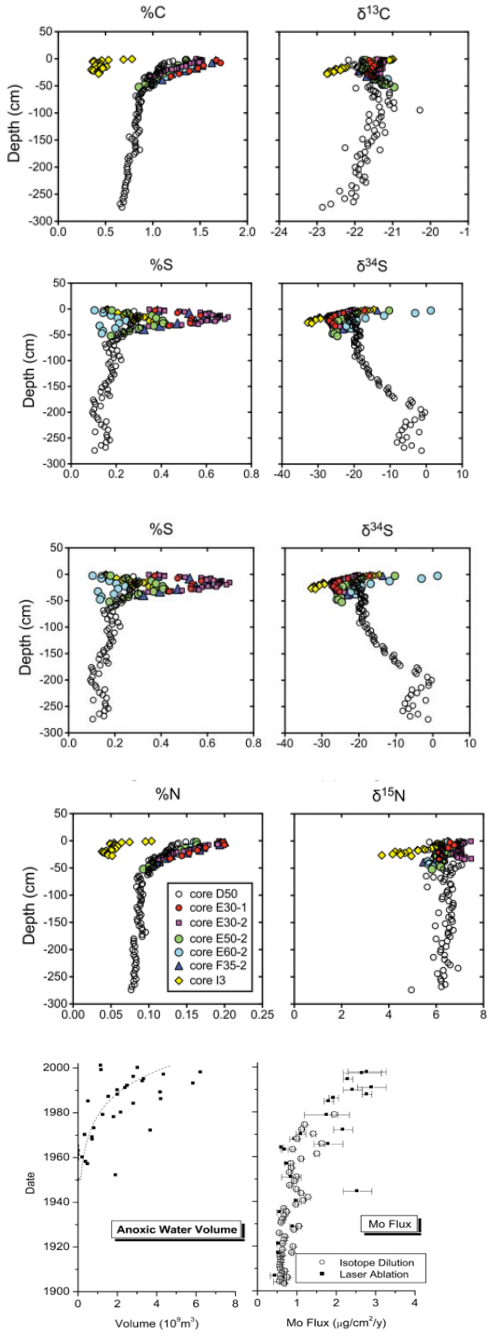

Figure 2. C, S, and N abundance and isotope composition of cores taken from the Mississippi Bight. Bottom figure shows Mo flux vs. volume of anoxic water through time in the Gulf of Mexico Dead Zone (Rabalais et al., 2014).

The Devonian-Mississippian transition in North America

During the Devonian-Mississippian transition in North America, the continent was flooded by a series of epicontinental seas. Anoxic deposition in the Appalachian Basin is represented by black shale units in present-day New York, Pennsylvania, Ohio, West Virginia, Virginia, Kentucky, and Tennessee. This tectonically-active foreland basin was shaped by the Acadian orogeny and was variably connected to the Rheic Ocean over the Cumberland Sill. The main black shale units in the Appalachian Basin are the Upper Devonian Ohio Shale, Lower Mississippian Sunbury Shale, and the Chattanooga Shale which covers a broader interval of Frasnian, Famennian, and Tournaisian time. The Illinois Basin is located to the west of the Appalachian Basin, separated by the Cincinnati Arch. Black shales from this basin are found in present-day Kentucky, Indiana, and Illinois. The main black shale unit from the Illinois Basin is known as the New Albany Shale.

To the northwest of the Illinois Basin, the Iowa Basin is bounded by the Sangamon Arch (Witzke et al., 1988). Black shale from this basin is found in Iowa and is also known as the New Albany Shale. The Michigan Basin is located to the northeast of the Illinois basin, beyond the Kankakee Arch (Ekblaw et al., 1938). Located in the present-day state of Michigan, the main black shale unit of interest is known as the Antrim Shale. The Anadarko Basin is situated southwest of the Illinois Basin beyond the Ozark Uplift. Black shales of this basin are located in modern-day Oklahoma, Kansas, and Texas, and the main unit is known as the Woodford Shale. The Permian Basin is located further southwest beyond the Anadarko Basin and is separated by the Amarillo-Wichita Uplift (Hammesch

et al., 2014). It is separated from the Rheic Ocean by the Concho Arch. Black shale units in this basin are located in Texas and New Mexico and are also known as the Woodford Shale (Commer, 1991). Beyond the Transcontinental Arch lies the Williston Basin. It is located in present-day Montana, North Dakota, and Saskatchewan. The black shale unit here is known as the Bakken Shale. Finally, the Pilot Basin is located furthest to the west proximal to the Panthalassa Ocean. It contains the Pilot Shale deposited across the Devonian-Mississippian transition.

Each of these basins were broadly characterized by the presence of anoxia and the production of black shales across the Devonian-Mississippian transition. This was likely the consequence of widespread global changes that resulted from the evolution of land plants. For the first time in Earth's history, large-scale development of soils stimulated by an increase in plant root depths created an influx of nutrients to global waters, including the North American intracratonic basins. The influx of nutrients likely led to eutrophication which, coupled with stratification of the water column, drove widespread anoxia in epicontinental seas (Algeo and Scheckler, 1998).

The advance of anoxia into more shallow waters coincides with mass extinction events. In the Late Devonian, a series of pulsed mass extinction events took place. The largest of these is known as the Kellwasser Event and took place around the Frasnian-Famennian boundary at ~372 Ma. It is separated into the Lower and Upper Kellwasser events (McGhee, 1996). Later, the Hangenberg Event occurred at ~359 Ma immediately prior to the Devonian-Mississippian boundary. These extinction events both dramatically effected marine vertebrate and invertebrate species, especially shallow-water taxa and

coral-stromatoporoid reef communities. Black shales deposited in the intracratonic basins of North America during the Devonian-Mississippian transition record direct evidence of the expansion of shallow-water euxinia, which may have been a primary kill mechanism in these extinction events. In addition to the Kellwasser and Hangenberg events, a series of smaller-scale anoxic and extinction events are recorded over >15 Ma of the Middle and Late Devonian. These include the Nehden, Condroz, Enkeberg, Annulata, and Dasberg events, among others. The samples analyzed in this project are not just relevant for the development of the uranium isotope redox proxy, but also because they record evidence of important events in Earth history.

The Appalachian Basin

Tectonic context

The Appalachian Basin is an intracratonic sedimentary basin that sits west of the Blue Ridge province and the associated metamorphic core of the Appalachian Mountains. It contains a thick succession of Paleozoic sedimentary rocks spanning from the Cambrian to the Pennsylvanian. The lithology and stratigraphic architecture of the Appalachian Basin is controlled by three major orogenic episodes of the Paleozoic: the Taconic, Acadian, and Alleghenian orogenies. The Taconic Orogeny occurred during the Middle-Late Ordovician due to an ocean island-arc colliding with the Laurentian plate (Faill, 1997). The Acadian Orogeny, which began in the Middle Devonian, lasted for ~50 Myr and reached its climax during the Late Devonian, setting the stage for the deposition of thick packages of siliciclastic strata in the Appalachian Basin (Ettensohn, 1985). During the Pennsylvanian

and Permian periods, the Alleghenian Orogeny developed as a result of Laurentia-Gondwana collision during the formation of Pangea (Hatcher, 2010). Throughout the Paleozoic Era, periods of tectonic quiescence were associated with carbonate platform development in the Appalachian Basin, whereas periods of tectonic activity were associated with large fluxes of clastic sediment into the basin. The period of interest in this study (Late Devonian-Early Mississippian) was characterized by active siliciclastic sediment flux during the Acadian Orogeny. During the Late Devonian-Early Mississippian, the Appalachian Basin was positioned at ~20º S paleolatitude.

Devonian-Mississippian stratigraphy

During the Middle Devonian to Early Mississippian, a shallow epicontinental sea flooded the Appalachian Basin. Siliciclastic sediment was sourced from a large delta complex (the Catskill Delta) that extended off the Acadian highlands into present-day New York and Pennsylvania (Ettensohn, 1985). The basin reached its deepest point (the foredeep of the active Acadian foreland basin) in the central Appalachians (present-day Ohio and West Virginia) before shallowing to the southwest into Kentucky and Tennessee towards the basin-bounding Cumberland Sill in central Tennessee. On the western side of the flooded Appalachian Basin, there was a regional topographic high (the Cincinnati Arch) west of which was another epicontinental sea in the intracratonic Illinois Basin. The stratigraphic units of interest were deposited during a series of transgressive and regressive events that took place during the Devonian and Mississippian periods. The Late Devonian (Famennian) organic-rich Huron Member of the Ohio Shale was deposited during a

transgressive episode under varying anoxic and suboxic conditions. The Huron Member is followed by the coarser-grained, greenish-grey, and pyrite-rich Three Lick Bed deposited during eustatic fall (Provo et al., 1977). Above the Three Lick Bed lies the Late Devonian (Famennian) organic-rich Cleveland Member of the Ohio Shale, which was deposited during another transgressive episode prior to the Devonian-Mississippian boundary. Above the Cleveland Member lies the Bedford-Berea complex, which represents progradation of coarser-grained facies across the basin during a dramatic fall in sea level across the Devonian-Mississippian boundary. This event is associated with a glaciation as evidenced by diamictites at many localities in Gondwana (Isaacson et al., 2008) and some in the Appalachian Basin (Brezinski et al., 2008). Following end-Devonian glaciation and deposition of the Bedford-Berea complex, rapid post-glacial transgression led to deposition of the Lower Mississippian (Tournaisian) organic-rich Sunbury Shale. Lastly, the Sunbury Shale is overlain by the organic-poor Cuyahoga Formation, associated with another eustatic fall.

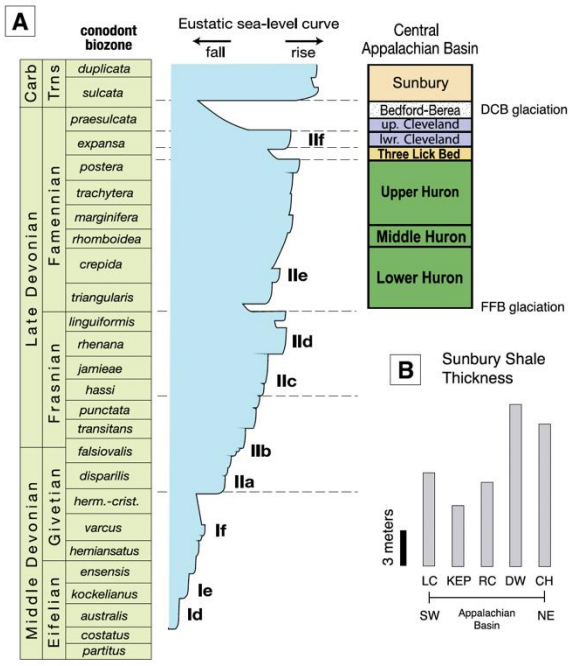

Figure 3. (A) Devonian-Mississippian stratigraphy of the Appalachian Basin with sea level history and conodont zonation. (B) Thickness of the Sunbury Shale in the five cores examined.

The Sunbury Shale

The focus of this study is the organic-rich Sunbury Shale, which ranges from ~6 to 16 meters thick in the study cores. The deposition of this black shale is suggested to be during the *sulcata* conodont Zone, which is the first biostratigraphic subdivision of the Tournaisian stage of the Early Mississippian (Sandberg et al., 2002). Some recent work, however, has suggested the Sunbury Shale may be slightly younger (beginning in the *duplicata* Zone and continuing through the *sandbergi* Zone) (Over, 2021). Regardless, its deposition is constrained to soon after the Devonian-Mississippian boundary, which is placed at 359.3 ± 0.3 Ma (Gradstein et al., 2020). Black shale and the lack of wave-induced sedimentary structures or noticeable influxes of sand or silt suggest deposition of the Sunbury Shale below storm wave-base in the central and southern Appalachian Basin. Some evidence for storm or wave activity is found closer to the Catskill Delta further to the north (Ettensohn, 1985).

Gamma-ray logs reveal, however, that several cycles of increasing and decreasing gamma response are present in the Sunbury Shale. In several wells from Ohio (see Fig. 3), there is a rapid spike in gamma response across the contact from the Bedford-Berea complex into the Sunbury Shale. This is then followed by a fall in gamma response and either one or two more rises and falls in gamma response before the contact with the overlying Borden Formation. In a well from Kentucky (see Fig. 3), there is a more gradual rise in gamma response across the contact from the Bedford-Berea complex into the Sunbury Shale. This is then followed by a fall and a second rise before a sharp drop into the overlying organic-poor unit. These cycles in gamma response could correspond to

broad eustatic cycles that are not recorded by distinct facies variations in these black shale units. Gamma responds to TOC content, the concentration of clays that contain radioactive K, and the concentration of Th and U, which is related to redox conditions. Oftentimes, maximum gamma response is linked to maximum transgression.

Devonian-Mississippian strata of the Appalachian Basin were subject to extensive physical deformation during Appalachian orogenic events, but the Sunbury Shale did not experience regional or contact metamorphism and organic matter is either immature or within the oil window (Schwark and Empt, 2006).

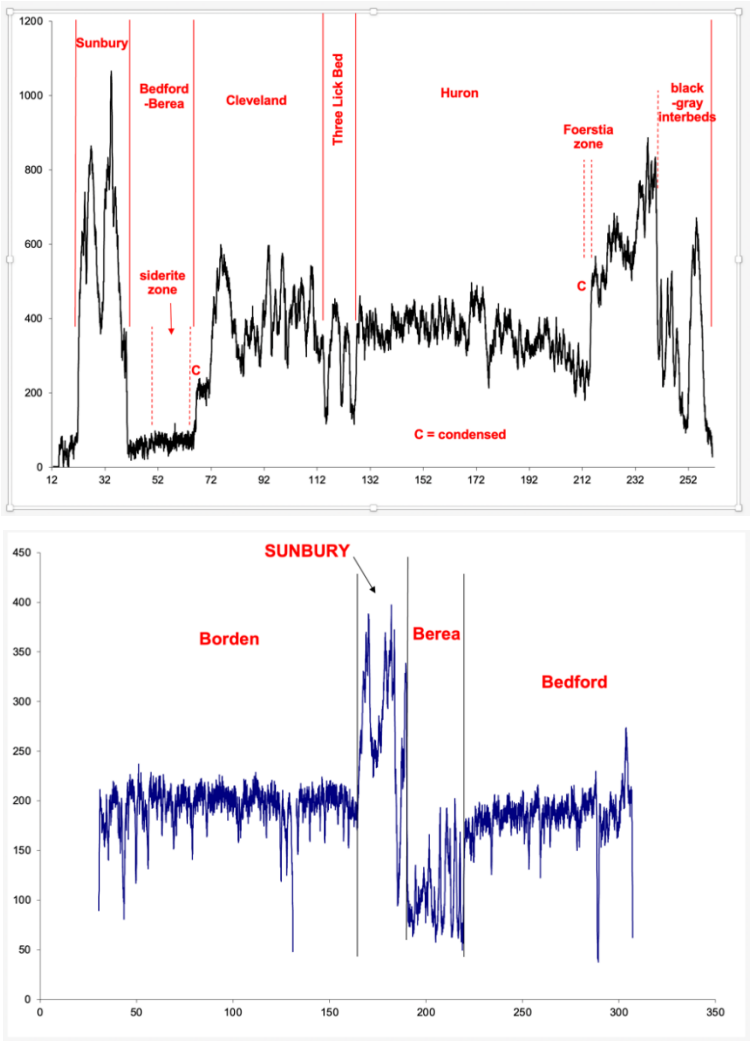

Figure 4. Spectral gamma logs for the KEP-6 core (Kentucky) (top) and OHRS4 core (Ohio) (bottom). Core depth in feet is on the x-axis and API units are on the y-axis. Lithostratigraphic units are indicated in red above the log.

METHODS

Uranium isotopes

Systematics

Uranium occurs in nature mainly as ^{238}U and ^{235}U isotopes. ^{238}U has a half-life of 4.468 Gyr and ^{235}U has a half-life of 700 Myr. U isotopes are expressed in delta notation ($\delta^{238}U$), which refers to the $^{238}U/^{235}U$ ratio of a sample compared to a standard reference material (CRM-145) with units of per mil (‰ or parts per thousand). In seawater, uranium exists as U(IV) and U(VI) oxidation states, which are insoluble and particle-reactive, and soluble, respectively. Isotopic fractionation occurs as U(VI) is reduced to U(IV), enriching U(IV) in ^{238}U and U(VI) with ^{235}U. In an anoxic water column, U(VI) is reduced to U(IV) and removed to sediment. This process removes ^{238}U from ocean water and leaves it enriched with ^{235}U, although this study aims to test which anoxic redox buffers produce which type of U isotope fractionation. Uranium has a residence time of 400 kyr in the modern oceans, which is longer than the ocean mixing time. The mean $\delta^{238}U$ value of modern seawater is -0.39 ± 0.01‰ and U is well-mixed across the oceans with a uniform open ocean concentration of ~3.2 ng/g (Tissot and Dauphas, 2015). The global homogeneity of seawater $\delta^{238}U$ means that its concentration and isotopic composition at any locality represent the global ocean.

Modern environments and experimental constraints

Uranium isotopes have been studied in a number of modern anoxic or low-oxygen basins that can inform the results of this study. Rolison et al. (2017) studied the modern Black Sea, which is a strongly restricted sub-basin of the Mediterranean Sea connected to the main watermass through the narrow Straits of Bosporus. In the central basin of the Black Sea, oxygen penetrates to ~100 m depth, below which environments are persistently euxinic. In deep waters below ~100 m depth, H_2S concentrations are >400 µM. Surface waters in the Black Sea have $\delta^{238}U$ values between −0.33 and −0.39‰, which is similar to the upper continental crust. Below the redoxcline, $\delta^{238}U$ values are between −0.60 and −0.86‰, suggesting removal of isotopically heavy U to sediments, leaving the residual watermass below the redoxcline with lower $\delta^{238}U$ values. By contrast, euxinic sediments in the Black Sea have $\delta^{238}U$ values between −0.2 and +0.2‰. These observations suggest an isotopic fractionation factor between water and sediment in the euxinic Black Sea of 0.63 to 0.84‰.

Holmden et al. (2015) studied another modern euxinic environment: the Saanich Inlet of British Columbia, Canada. In the Saanich Inlet, oxygen penetrates to between 120 and 150 m depth, below which environments are persistently euxinic. Seasonally in the fall, freshwater mixes into the Strait of Georgia, allowing oxygenated waters to penetrate lower in the water column. Water in the Saanich Inlet has a uniform $\delta^{238}U$ value averaging −0.45 ± 0.04‰ throughout the water column down to 200 m. By contrast, authigenic U in euxinic sediments and sediment trap samples in the Saanich Inlet have an average $\delta^{238}U$ value of +0.17‰. These observations suggest an isotopic fractionation factor between

water and sediment in the euxinic Saanich Inlet of 0.62 ± 0.17‰ (2σ). This is in good agreement with what was observed in the Black Sea, suggesting that euxinic environments may be characterized by a common fractionation factor during U(VI) reduction to U(IV).

Additionally, Kaltenbach (2012) studied U isotope fractionation in the strongly euxinic Framvaren Fjord of Norway. In the Framvaren Fjord, oxygen penetrates to 18 m depth, below which environments are persistently euxinic. In waters below 100 m depth, H_2S concentrations increase from around 3000 µM to greater than 4500 µM. In contrast to the Black Sea and Saanich Inlet where U(VI) reduction to U(IV) is thought to occur at or below the sediment-water interface, in the Framvaren Fjord there is active U(VI)-reduction and thus isotopic fractionation occurring in the strongly euxinic water column. Water in the Framvaren Fjord has a $\delta^{238}U$ value of −0.45‰ at 10 m depth above the redoxcline, but progressively drops to −0.81‰ at 40 m depth below the redoxcline, suggesting that again, reduction of U(VI) to U(IV) results in preferential removal of the heavy ^{238}U isotope. No sediments have been measured in the Framvaren Fjord to assess fractionation during sedimentation. These observations suggest that, once again, euxinic environments strongly fractionate U isotopes.

Although a number of studies have focused on modern euxinic environments, relatively few have examined ferruginous environments, which are less abundant on Earth's surface. Cole et al. (2020) examined both oxic and ferruginous sediments from stratified Lake Pavin (France) and Brownie Lake (Minnesota). In Brownie Lake, the average $\delta^{238}U$ value of oxic sediments was −0.15‰ and the average $\delta^{238}U$ value of ferruginous sediments was −0.07‰. This suggests minimal isotopic fractionation during U

removal to ferruginous sediments. In Lake Pavin, the average $\delta^{238}U$ value of oxic sediments was −0.37‰ and ferruginous sediments showed a wide range of $\delta^{238}U$ values from −0.81 to +0.30‰. The authors attributed this large range of $\delta^{238}U$ values in ferruginous sediments to abiotic reduction with ferrous iron, sorption of U to iron oxides, and vivianite providing an alternate pathway for U reduction.

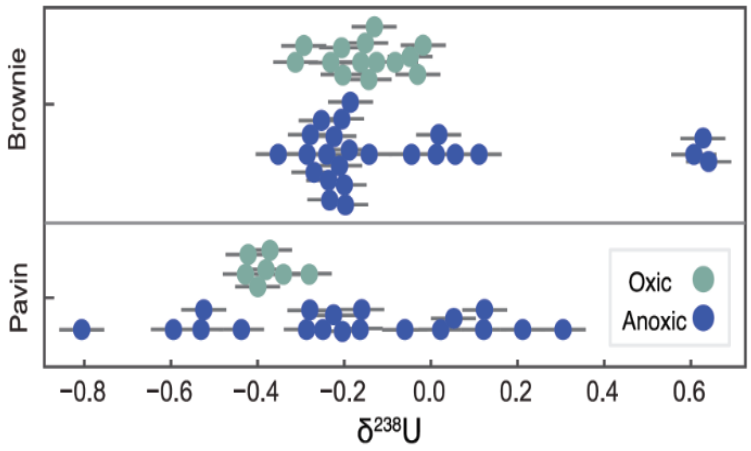

Figure 5. Uranium isotope compositions of oxic and ferruginous sediments from Brownie Lake (Minnesota) and Lake Pavin (France). Both the oxic and ferruginous redox environments produce similar fractionation in these two settings (Cole et al., 2020).

Gilleaudeau et al. (in prep) also investigated U isotopes in water and sediments of stratified, ferruginous Canyon Lake (Michigan). Here, the entire water column, oxic sediments, and ferruginous sediments showed an identically tight range of $\delta^{238}U$ values

near −0.4‰, similar to the upper continental crust. Together, these data suggest a lack of U isotope fractionation during U(VI) reduction under ferruginous conditions. There have also been experiments performed investigating U(VI) reduction in the presence of a variety of Fe-based reductants including $Fe(II)_{aq}$, green rust, and magnetite (Stylo et al., 2015). Counterintuitively, these experiments showed the preferential removal of isotopically-light ^{235}U during reduction, leaving the solution with progressively higher $\delta^{238}U$ values. In summary, existing data suggest that U isotopes show a lower and more variable degree of fractionation under ferruginous conditions, which may be attributed to a variety of factors. This is in contrast to the larger degree of isotopic fractionation that occurs in euxinic waters, where there is strong preferential removal of the heavy ^{238}U isotope during U reduction.

In addition to redox conditions at the sediment-water interface, two recent studies identified additional factors that may affect the degree of isotopic fractionation expressed during U removal in low-oxygen settings. Bruggmann et al. (2022) looked at U removal to sediments in the highly productive, modern Peruvian upwelling zone. Upwelling at the Peruvian margin is caused by winds traveling northwestward, parallel to the continent. Ekman transport pushes surface water away from the coast and bottom water moves in to replace it. Upwelling causes high rates of primary productivity, resulting in sediment TOC concentrations up to 20 wt.%. Anoxic conditions are generated and sustained due to the decomposition of organic material throughout the water column. In contrast to restricted basins such as the Black Sea, anoxic waters of the Peruvian upwelling zone are non-euxinic. The concentration of H_2S is not great enough to permeate the water column above the sediment-water interface.

Bruggmann et al. (2022) looked at sediment cores spanning from the oxic shelf through the anoxic portion of the oxygen minimum zone (OMZ) and down to below the OMZ when oxygen concentrations rise again. Oxic sediment samples from the Peruvian margin have authigenic $\delta^{238}U$ values between −0.34 and −0.25‰, indicating a fractionation factor between authigenic sediment and seawater of between 0.05 and 0.14‰. In contrast, anoxic and non-euxinic sediments have authigenic $\delta^{238}U$ values between −0.34 and +0.01‰, indicating a fractionation factor between authigenic sediment and seawater of 0.07 to 0.40‰. This fractionation factor is higher and more variable than seen in oxic sediments from the same Peruvian margin but is overall lower than has been observed in modern euxinic settings (i.e., the Black Sea, Saanich Inlet, and Framvaren Fjord; see above). In addition, Bruggmann et al. (2022) found strong correlations between sediment $\delta^{238}U$ values and TOC. In the anoxic core from the center of the OMZ, linear regression of sediment $\delta^{238}U$ and TOC produces an R^2 value of 0.94. Bruggmann et al. (2022) suggest reasons for the strong correlation between $\delta^{238}U$ and TOC. Particulate and diffusive input of U can change sediment U isotopic composition and concentration. TOC affects the level of microbially-mediated U reduction, the amount of adsorbed U delivered to the sediment along with organic matter, and diagenetic redistribution of U. In summary, Bruggmann et al. (2022) suggest that organic carbon rain and burial rates strongly influence sediment $\delta^{238}U$ values, in addition to bottom-water redox conditions.

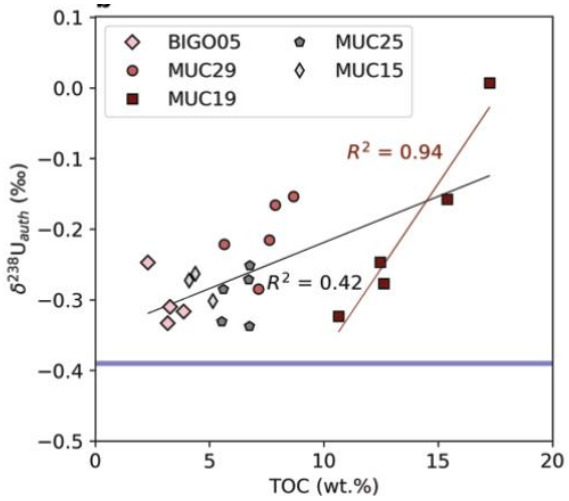

Figure 6. Uranium isotopes plotted versus TOC in sediments from the modern Peruvian Margin. There is a strong correlation between $\delta^{238}U$ and TOC specifically in permanently anoxic sediments from the core of the OMZ (core

Lau et al. (2022) investigated U isotopes in two basins (Santa Barbara and San Joaquin) of the Miocene Monterey Formation. The Monterey Formation was deposited between 6 and 18 Ma along the west coast and interior of central California. The San Joaquin Basin is located in central California, while the Santa Barbara Basin sits along the west coast. They are separated by the San Andreas Fault. The Monterey Formation is comprised of three general members: Early Miocene calcareous-siliceous mudstone, Middle Miocene organic-rich marlstone, and Middle to Upper Miocene siliceous mudstone. Local redox conditions during the deposition of the Monterey Formation

differed between basins. The San Joaquin Basin was dominated by euxinic waters, while the Santa Barbara Basin was dominantly anoxic, with intermittent periods of euxinia. The Santa Barbara Basin experienced upwelling that led to high organic carbon loading. Lau et al. (2022) sampled two shale cores from the San Joaquin and Santa Barbara basins to measure $\delta^{238}U$. The Thorndyke core taken from the San Joaquin Basin had a mean $\delta^{238}U$ value of −0.14‰, while the Naples Beach section taken from the Santa Barbara Basin had a mean $\delta^{238}U$ value of −0.05‰. Lau et al. (2022) also investigated coeval Miocene carbonates in order to approximate the U isotope composition of Miocene seawater. These carbonates were taken from ODP Leg 166 (Great Bahama Bank) and Leg 194 (Marion Plateau, Great Barrier Reef). Their dominant mineralogy is calcite, with minor occurrences of dolomite and non-carbonate minerals. $\delta^{238}U$ values from Leg 194 have a mean of −0.25‰ and values from Leg 166 have a mean of −0.17‰ with greater variance. Using these data to estimate the Miocene seawater $\delta^{238}U$ composition, this suggests a fractionation factor of +0.36‰ in the euxinic San Joaquin Basin and a fraction factor of +0.44‰ in the anoxic, highly productive Santa Barbara Basin. These results suggest that both euxinic and non-euxinic, anoxic settings can strongly fractionate U isotopes, and that the degree of fractionation is dependent on local factors such as productivity, sedimentation rates, persistence of anoxia, phosphate content, and basin hydrography.

Laboratory procedures

In order to prepare samples for U isotope analysis, a series of steps were taken to isolate the U from matrix elements. ~120 mg of powdered sample was first ashed in a muffle furnace at 550 °C overnight. This procedure was previously performed at the

University of Maryland for an initial set of samples and at George Mason University for the remainder of samples. This procedure is designed to remove organic matter and volatiles. Ashed powders were then placed in clean Teflon beakers in preparation for digestion. 5 mL of concentrated trace-metal-grade HNO_3 and 1 mL of concentrated trace-metal grade HF were added to the powder in order to begin dissolution. Between each phase of digestion, the solutions in the Teflon beakers were dried on a hot plate. After the beakers cooled, 2 mL of concentrated trace-metal-grade HCl was added. Once the solution was sufficiently dried down and the beakers cooled again, 5 mL of 6 M trace-metal-grade HCl and 2 drops of concentrated trace-metal-grade HF were added to each beaker. After a final dry down, samples were dissolved in 10 mL of 3 M HNO_3 for column chemistry.

Uranium was separated from matrix elements by ion exchange chromatography using UTEVA resin. After column chemistry, separated U was treated twice with concentrated $HNO_3 + H_2O_2$ to remove any residual organics from the resin. Purified U was then dissolved in an appropriate amount of 2% HNO_3 to produce a solution with 50 ppb U. The purified U solution was measured for its isotopic composition using a Neptune Plus multi-collector ICP-MS at the University of Maryland. Measured $^{238}U/^{235}U$ ratios were normalized to the CRM-145 standard using sample-standard bracketing, and each sample was run 2-4 times to ensure analytical precision. Analytical precision is reported as 2 s.d. of replicate measurements. The viability of the U isotope methodology at the University of Maryland has been verified in a series of inter-laboratory comparison studies conducted by advisor Gilleaudeau (see Cherry et al., in press).

Iron speciation

Fe_{HR}, Fe_{py}, Fe_T, and differentiating redox environments

Iron speciation was used to distinguish local redox conditions during deposition of the Sunbury Shale across the cores examined in this study. This technique quantifies the amount of Fe in each mineralogical phase of shales, which is highly dependent on local redox conditions. Highly reactive iron (Fe_{HR}) is the sum of iron phases that are reactive to sulfide during early diagenesis and include iron carbonate, iron oxyhydroxides, magnetite, iron-rich clay minerals, as well as pyrite (Fe_{py}) which is the product of that reaction (Raiswell and Canfield, 1998). In anoxic conditions, sediment is enriched in Fe_{HR} relative to total iron (Fe_T). This occurs because of the addition of authigenic iron minerals from the water column (Lyons and Severmann, 2006). Fe_{HR}/Fe_T values above 0.38 represent anoxic conditions (Raiswell and Canfield, 1998). Fe_{HR}/Fe_T values below 0.22 are indicative of an oxic setting. Fe_{HR}/Fe_T values between 0.22 and 0.38 are considered potentially anoxic or equivocal (Poulton and Canfield, 2011).

The presence of specific iron minerals in a sample can also be used to determine if it was deposited under ferruginous or euxinic conditions. Euxinic environments are enriched in pyrite, while ferruginous settings are dominated by iron carbonate, iron oxyhydroxides, magnetite, and iron-rich clay minerals. Data from modern anoxic basins show that Fe_{py}/Fe_{HR} ratios above 0.8 indicate euxinic conditions, while Fe_{py}/Fe_{HR} ratios below 0.8 indicate ferruginous conditions (Anderson and Raiswell, 2004). Other studies put the cutoff value at 0.7 (März et al., 2008). Iron speciation has been widely used to study redox throughout Earth history. It was used to determine ocean redox conditions and the

variable advance of euxinia in the water column during the Proterozoic (Poulton et al., 2010). Iron speciation data were also used to understand the retreat of anoxic conditions during the Ediacaran Period associated with the rise of animals (Bowyer et al., 2020).

Laboratory procedures

Iron speciation analyses were conducted at the University of California, Riverside, following published methods (Poulton and Canfield, 2005). Pyrite iron (Fe_{py}) was calculated (assuming a stoichiometry of FeS_2) from the mass of Ag_2S precipitated during a two-hour hot chromous chloride distillation (Canfield et al., 1986). Other iron species—specifically, Fe_{carb}, Fe_{ox}, and Fe_{mag}—were extracted sequentially (Poulton and Canfield, 2005). ~100 mg of sample powder was first reacted with a 1 M sodium acetate solution buffered with acetic acid to a pH of 4.5. The extraction lasted for 48 hours. After decanting the solution, the sample powder was then subjected to a 50 g/L sodium dithionite solution buffered with 0.35 M acetic acid and 0.2 M sodium citrate to a pH of 4.8. The extraction lasted for two hours. Lastly, after decanting the previous solution, the sample powder was subjected to a 0.2 M ammonium oxalate, 0.17 M oxalic acid solution buffered to a pH of 3.2. The extraction lasted for six hours. These three solutions are designed to extract Fe_{carb}, Fe_{ox}, and Fe_{mag}, respectively. The ammonium oxalate solution has also been shown to extract iron-rich clay minerals (Slotznick et al., 2020). Iron concentrations in each extraction solution were measured using the ICP-MS at the University of California, Riverside. Fe_T was determined using HF-HNO_3-HCl acid digestion. About 100 mg of sample was ashed at 550 °C and sequentially digested in pre-cleaned Savillex Teflon

beakers using HF-NHO_3, aqua regia (HNO_3-HCl), and finally HCl. Final solutions were diluted 100-fold with trace metal grade 2% HNO_3 and analyzed using an ICAP-Q quadrupole ICP-MS at Arizona State University. Reproducibility of iron measurements, monitored by duplicate analyses, was better than 5% (2σ).

Previous watermass reconstruction

In this study, we propose to analyze U isotopes in the Sunbury Shale in five drill cores across the Appalachian Basin. They range from environments proximal to the Catskill Delta complex in northeastern Ohio (the CH core), to environments in the deep central axis of the Appalachian Basin in central and southern Ohio (the DW and RC cores), to environments that shoaled towards the basin-bounding Cumberland Sill in eastern Kentucky (the KEP and LC cores). The CH core is taken from Cuyahoga County, Ohio (near Cleveland) at 41.440°N, 81.564°W. The DW core is taken from Delaware County, Ohio (near Harlem) at 40.203°N, 82.805°W. The RC core is taken from Ross County, Ohio (near Huntington) at 39.258°N, 83.076°W. The KEP core is taken from Lewis County, Kentucky at 38.409°N, 83.437°W. The LC core is taken from Leslie County, Kentucky at 37.156°N, 83.389°W. Further details can be found in Gilleaudeau et al. (2021).

Figure 7. Paleogeographic map of North America at 360 Ma with inset showing location of five cores examined in this study (Gilleaudeau et al., 2021).

Cores were previously logged onsite by G. Gilleaudeau and T. Algeo and samples were collected using a diamond-blade saw. Rocks were previously crushed and powdered using a steel ball mill at the University of Cincinnati. Samples from all five cores were previously analyzed for paleo-redox conditions using total organic carbon (TOC) and sulfur, TOC/P ratios, iron speciation, trace metal abundances, and pyrite sulfur isotopes (Gilleaudeau et al., 2021). In the CH core deposited in proximal environments close to the Catskill Delta, Fe_{HR}/Fe_T ratios between 0.22 and 0.38 show ambiguous redox conditions, but TOC and TOC/P ratios are low and trace metal concentrations are near crustal values. This indicates oxic conditions, possibly due to shallow water deposition and freshwater

coming off the delta that deepened the regional pycnocline. In the DW and RC cores, TOC, TOC/P ratios, and trace metals are substantially higher than the CH core. These cores were deposited deeper in the central axis of the basin. Iron speciation indicates ferruginous conditions, with Fe_{HR}/Fe_T ratios above 0.38 and Fe_{py}/Fe_{HR} ratios below 0.8. The KEP and LC cores were deposited as environments shoaled towards the Cumberland Sill in the south. Both iron speciation ratios (Fe_{HR}/Fe_T and Fe_{py}/Fe_{HR}) are high, which shows the development of euxinic conditions. Trace metals are strongly enriched in both cores, and TOC and TOC/P ratios reach their highest levels in the KEP core (Gilleaudeau et al., 2021).

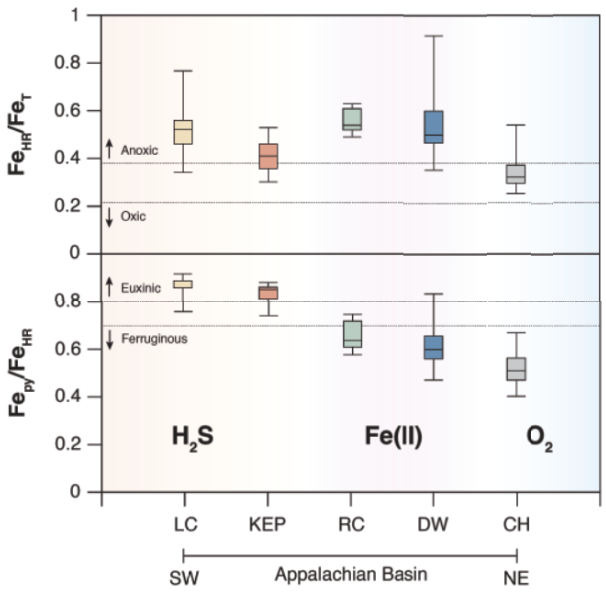

Figure 8. Box and whisker plot showing iron speciation data from the five cores of interest. Note oxic conditions in the CH core, ferruginous conditions in the DW and RC cores, and euxinic conditions in the LC and KEP cores (Gilleaudeau et al., 2021).

Using these proxy data, we conclude that redox conditions in the Appalachian Basin were variable laterally from the Catskill Delta in the northeast to environments approaching the open Rheic Ocean beyond the Cumberland Sill to the southwest. These redox conditions are generally characterized by oxic surface water with a euxinic region below the redoxcline, and ferruginous conditions located at the deepest sections along the central basin axis. Freshwater influx from the Catskill Delta deepened the redoxcline and allowed for more oxic conditions to reach the CH core. Ferruginous bottom waters prevailed towards the central basin axis where the DW and RC cores were logged. In contrast, the KEP and LC cores taken from shallower-water environments towards the Cumberland Sill show euxinic conditions (Gilleaudeau et al., 2021). Together these data indicate a strong lateral redox gradient across the Early Mississippian Appalachian Seaway, with oxic conditions in the northeastern-most CH core, ferruginous conditions in the deeper central axis of the basin (DW and RC cores), and euxinic conditions shoaling to the south (KEP and LC cores). This lateral redox gradient makes the Sunbury Shale an excellent test case for understanding U isotope fractionation under different redox conditions.

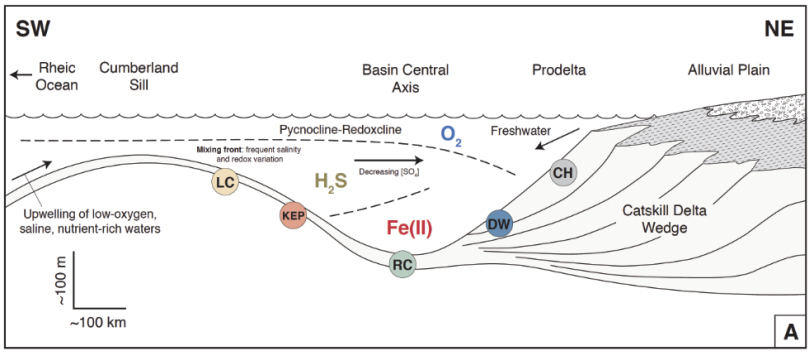

Figure 9. Reconstruction of Appalachian Basin watermass redox and salinity during deposition of the Lower Mississippian Sunbury Shale. Note the deepening of the oxic layer closer to the Catskill Delta. Variable mixing of waters from the Rheic Ocean occurred over the Cumberland Sill (Gilleaudeau et al., 2021).

It is also important to consider the salinity and degree of connectivity between the Appalachian Seaway and the open ocean during the Early Mississippian. This could influence the baseline $\delta^{238}U$ values in the area that each core was deposited in. Wei and Algeo (2020) proposed three elemental proxies for paleosalinity: the ratios of S/TOC, Sr/Ba, and B/Ga. S/TOC ratios >0.1 in all Sunbury Shale units indicate that freshwater conditions were not present in any of the five core sites (Gilleaudeau et al., 2021). Sr/Ba ratios generally between 0.2 and 0.5 indicate brackish salinities, however, across all five core sites during the Early Mississippian (Gilleaudeau et al., 2021). In addition, a salinity gradient was identified between low-brackish conditions in the northeastern-most CH core to higher-brackish conditions as you approach the Cumberland Sill and open ocean to the

southwest. The southwestern-most LC core shows the highest degree of salinity variation, suggesting that it was deposited in a shallow mixing zone along the edge of the Cumberland Sill where low salinity water from the Catskill Delta frequently mixed with incoming seawater from the open Rheic Ocean (Gilleaudeau et al., 2021). B/Ga was not measured in the Sunbury Shale samples, but a similar salinity gradient was shown using B/Ga in the Upper Devonian Cleveland Shale of the Appalachian Basin (Gilleaudeau et al., in prep), suggesting that brackish conditions and salinity gradients characterized the Appalachian Basin across the Devonian-Mississippian transition.

HYPOTHESES

We hypothesize that U isotope fractionation will be controlled by local redox conditions with the lightest U isotope values in the oxic CH core, intermediate U isotope values in the ferruginous DW and RC cores, and the heaviest U isotope values in the KEP and LC cores. There will be a strong relationship between iron speciation and U isotope values. The null hypothesis is that U isotope compositions will show no relationship to local redox conditions as recorded by iron speciation. The alternative hypothesis is that U isotope compositions will depend on local factors other than bottom-water redox, such as primary productivity and organic carbon loading. This is similar to conditions seen in the modern Peruvian upwelling zone and the Miocene Monterey Formation.

RESULTS

32 samples from the Sunbury Shale were subjected to a full chemical digestion and separation in two batches, first in December 2021 and then in September 2022 at GMU. These included 6 samples from the CH core, 5 from the DW core, 5 from the RC core, 7 from the KEP core, and 9 from the LC core. This also included 8 samples with an oxic to equivocal iron speciation signal, 10 samples with a ferruginous iron speciation signal, and 12 samples with an euxinic iron speciation signal. Two samples had no iron speciation data. The resulting solutions were measured for U isotopes at the University of Maryland by advisor Gilleaudeau in two sessions, March 2022 and October 2022. The analyses were successful and produced an average 2 s.d. for the dataset of 0.07‰, indicating a high degree of analytical precision comparable to published studies and our previous analyses at the University of Maryland (e.g., Gilleaudeau et al., 2019; Cherry et al, in press). In the CH core, U isotope values ranged from −0.37 to 0.00‰. In the DW core, they ranged from −0.05 to +0.57‰ and in the RC core, they ranged from −0.04 to +0.33‰. The KEP core ranged from +0.04 to +0.59‰ and the LC core ranged from −0.03 to +0.44‰. When considering all five cores, oxic to equivocal samples based on iron speciation showed U isotope values ranging from −0.37 to +0.08‰, whereas ferruginous samples ranged from −0.04 to +0.57‰ and euxinic samples from −0.05 to +0.59‰.

DISCUSSION

Modern analogues for the Early Mississippian Appalachian Seaway

The Early Mississippian Appalachian Basin shares common characteristics with modern analogues, as well as some key differences. The Appalachian Basin is similar to the modern Gulf of Mexico because both were fed by a large river system entering the basin (the Mississippi and Catskill deltas, respectively). Both of these basins can be split into zones that are more or less effected by local controls like freshwater influx and mixing. The Appalachian Basin was an active foreland basin that only reached several hundred meters deep. However, the Gulf of Mexico is much deeper than the Appalachian Basin, as it is situated on an open shelf, reaching several thousand meters depth in some areas. The Gulf of Mexico also has mostly marine salinities, while the Appalachian Basin had a brackish salinity. Still, in both scenarios, anoxia is driven by eutrophication and is related to nutrient runoff. In the case of the Gulf of Mexico, anoxia only exists in the shallowest parts of the water column proximal and to the west of the Mississippi Delta. In the Appalachian Basin, however, anoxia was persistent in the deeper parts of the basin, likely because of water column stratification. Similarities are also seen between the Chesapeake Bay and Appalachian Basin. Both have brackish salinities, salinity gradients, and shallow mixing. The Chesapeake Bay does not have as large of a delta complex, however, and is much shallower than the Appalachian Basin, with an average depth of only 7 meters. The Baltic Sea may be the best analogue for the Early Mississippian Appalachian Seaway

because they have a comparable depth and salinity gradient (Gilleaudeau et al., 2021). U isotope measurements in the Baltic Sea would be an important future direction for research.

Relationship between iron speciation and U isotope fractionation in the Sunbury Shale

Both the ferruginous and euxinic samples show strong fractionations towards heavier U isotope values, whereas oxic/equivocal samples from the CH core show the lowest U isotope values. The lowest degrees of fractionation associated with potentially oxic environments is expected given the lack of U(VI) reduction to U(IV) seen in these environments, with this process known to drive large U isotope fractionations. It is important to note, however, that iron speciation data do not unequivocally suggest oxic conditions in the CH core. In the six samples we analyzed from the CH core, TOC ranges between 0.6 wt.% (which is more typical of oxic conditions) and 2.1 wt.% (which is typically only possible under suboxic to anoxic conditions). It is therefore likely that some U(VI) to U(IV) reduction was occurring in environments represented by the CH core, thus explaining U isotope values up to 0‰, which is substantially higher that modern seawater (and likely Tournaisian seawater; see discussion below) and higher than would be expected for purely oxic environments. Based on the data for unequivocally anoxic samples (Fe_{HR}/Fe_T > 0.38), however, U isotope values do not seem to depend on local redox conditions as recorded by iron speciation (i.e., whether samples were deposited under euxinic or ferruginous conditions). Ferruginous and euxinic samples show little difference in U isotope fractionation. Based on this, U isotope values are not as strongly dependent

on euxinic vs. ferruginous conditions as initially expected and as has been previously suggested (Cole et al., 2020).

We can also compare our data from the Sunbury Shale to carbonates deposited at roughly the same time to truly assess the degree of U isotope fractionation between samples from the Sunbury Shale and coeval seawater. Carbonates have the ability to record seawater U isotope values with a relatively minor offset of 0.3‰ of less under most conditions (Chen et al., 2018). Specifically, carbonates typically have higher $\delta^{238}U$ values than coeval seawater by ~0.3‰ because of authigenic addition of isotopically-heavy U(IV) under conditions of pore water anoxia (Romaniello et al., 2013; Chen et al., 2018). This offset seems to be remarkably consistent, however, regardless of burial depth and mineralogy along the modern Bahamian carbonate platform (Chen et al., 2018). Thus, we can apply a correction from carbonate $\delta^{238}U$ values back to the original seawater composition. Cheng et al. (2020) investigated the $\delta^{238}U$ composition of Lower Mississippian carbonates from southern Nevada (Antler foreland basin). These analyses comprised the Joana Limestone and Limestone X deposited during the Tournaisian stage. Specifically, the base of the Joana Limestone was potentially deposited during the *sanbergi* conodont Zone (Cheng et al., 2020), which is the same zone that is potentially recorded in the upper part of the Sunbury Shale (Over, 2021). Within the *sanbergi* conodont Zone in the Joana Limestone, $\delta^{238}U$ values along a LOESS fit through the data range from approximately −0.40 to −0.25‰ (Cheng et al., 2020). Applying a correction of 0.3‰ to these carbonate data, we estimate that Tournaisian seawater during the *sanbergi* conodont Zone had a $\delta^{238}U$ composition between −0.70 to −0.55‰. This is substantially lower than

the modern seawater value of −0.39‰, indicating expanded marine anoxia compared to today. Based on this estimate, the $\Delta^{238}U$ value ($\delta^{238}U_{sample} - \delta^{238}U_{seawater}$) can be calculated.

For samples with an oxic to equivocal iron speciation signal, potential $\Delta^{238}U$ values range from 0.18‰ (which is typical of oxic environments today) to 0.70‰ (which is much higher than is seen in modern oxic environments). One reason samples from the CH core could have higher $\delta^{238}U$ values than Tournaisian seawater despite some being deposited under potentially oxic conditions is that the CH core site was located proximal to freshwater runoff from the Catskill Delta in the northeastern part of the Appalachian Basin. Major modern rivers today have $\delta^{238}U$ values of approximately −0.30‰, which is similar to the upper continental crust (Tissot and Dauphas, 2015). Thus, using our Tournaisian seawater estimate to calculate $\Delta^{238}U$ values may not be appropriate for the CH core. This is evidenced by the CH core having the lowest values for Sr/Ba (average = 0.22), which is a paleosalinity proxy that, in this case, indicates low-brackish conditions at the CH study site. The higher-than-expected $\delta^{238}U$ values in the CH core could also indicate that environments were not fully oxic and that some U(VI) to U(IV) reduction was occurring, driving U isotope fractionation. This is evidenced by TOC values up to 2.1 wt.% in some samples. This relationship with TOC is explored further below.

For samples with a ferruginous iron speciation signal, potential $\Delta^{238}U$ values range from 0.51 to 1.27‰. This is a higher degree of fractionation that what was observed in modern ferruginous Canyon Lake (Gilleaudeau et al., in prep) and Brownie Lake (Cole et al., 2020). Canyon Lake and Brownie Lake are both oligotrophic lakes with low rates of primary productivity and organic carbon loading, which could explain the lower degree of

U isotope fractionation compared to ferruginous parts of the Appalachian Basin, where high TOC contents clearly indicate high productivity and organic carbon loading. For samples with a euxinic iron speciation signal, $\Delta^{238}U$ values range from 0.50 to 1.29‰, a nearly identical range to the ferruginous samples. This degree of fractionation is consistent with observations from modern euxinic environments such as the Black Sea, Saanich Inlet, and Framvaren Fjord, confirming that euxinic settings can impart a large degree of U isotope fractionation. Overall, we find that for anoxic samples, there is little to no relationship between iron speciation (i.e., ferruginous vs. euxinic conditions) and $\delta^{238}U$ or $\Delta^{238}U$ values, suggesting that factors other than bottom-water redox conditions are controlling the degree of U isotope fractionation.

For samples with a ferruginous iron speciation signal, potential $\Delta^{238}U$ values range from 0.51 to 1.27‰. This is a higher degree of fractionation that what was observed in modern ferruginous Canyon Lake (Gilleaudeau et al., in prep) and Brownie Lake (Cole et al., 2020). Canyon Lake and Brownie Lake are both oligotrophic lakes with low rates of primary productivity and organic carbon loading, which could explain the lower degree of U isotope fractionation compared to ferruginous parts of the Appalachian Basin, where high TOC contents clearly indicate high productivity and organic carbon loading. For samples with a euxinic iron speciation signal, $\Delta^{238}U$ values range from 0.50 to 1.29‰, a nearly identical range to the ferruginous samples. This degree of fractionation is consistent with observations from modern euxinic environments such as the Black Sea, Saanich Inlet, and Framvaren Fjord, confirming that euxinic settings can impart a large degree of U isotope fractionation. Overall, we find that for anoxic samples, there is little to no

relationship between iron speciation (i.e., ferruginous vs. euxinic conditions) and $\delta^{238}U$ or $\Delta^{238}U$ values, suggesting that factors other than bottom-water redox conditions are controlling the degree of U isotope fractionation.

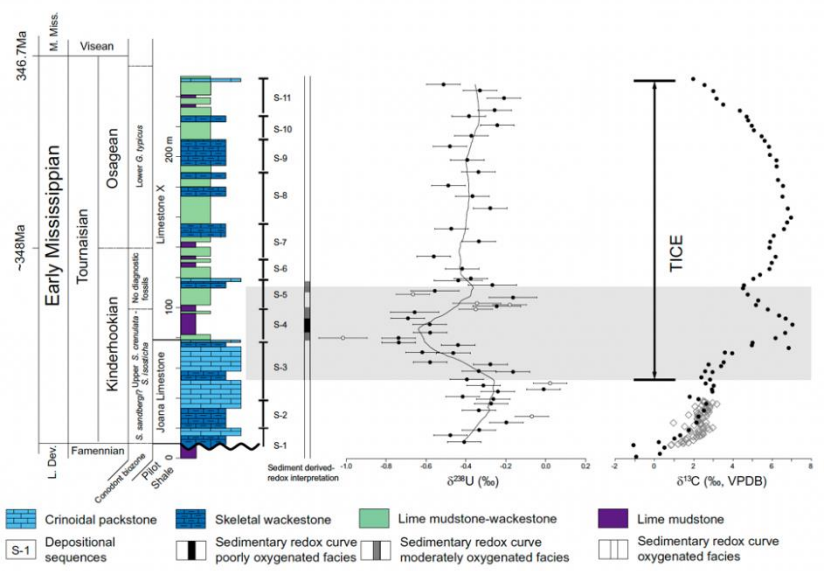

Figure 10. Carbonate U and C isotope profile through Lower Mississippian carbonates of the Joana Limestone and Limestone X, Nevada (Cheng et al., 2020).

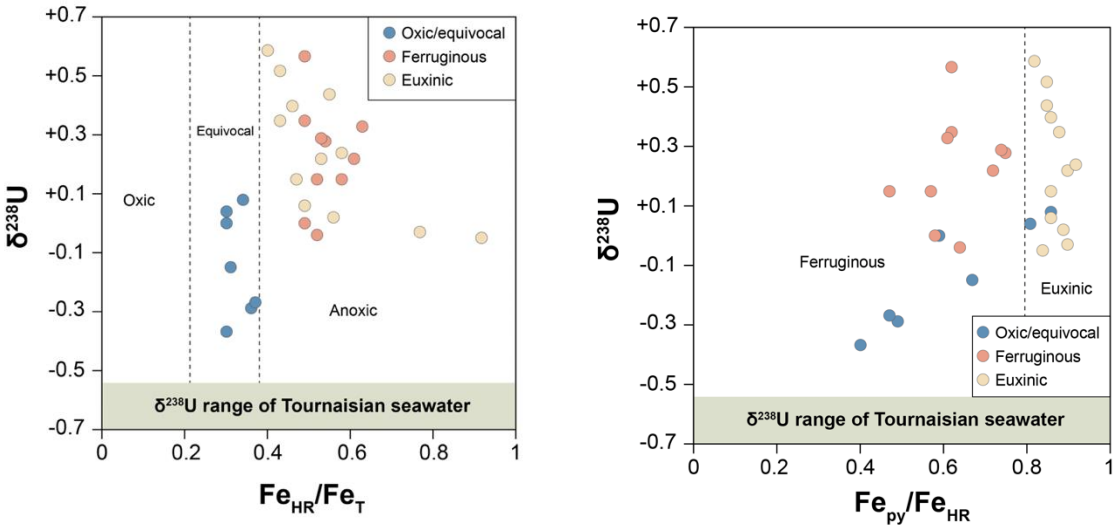

Figure 11. U isotope values vs. Fe speciation ratios in samples analyzed from the Sunbury Shale. Samples are color-coded by Fe speciation signal and the U isotope range of Tournaisian seawater comes from the coeval carbonates from Nevada.

Relationship between TOC, trace metal abundances, and U isotope fractionation

We also tested the relationship between $\delta^{238}U$ values and the abundances of TOC and select redox-sensitive transition metals in the Sunbury Shale samples. Plotting $\delta^{238}U$ vs. TOC, Mo, V, U, Ni, Zn, and Re concentrations using a linear regression produced a wide range of R^2 values (0.28 for TOC, 0.49 for Mo, 0.55 for V, 0.28 for U, 0.41 for Ni, 0.35 for Zn, and 0.19 for Re). Interestingly, these R^2 values increase substantially, however, when using a logarithmic regression line (0.52 for TOC, 0.64 for Mo, 0.68 for V, 0.45 for U, 0.58 for Ni, 0.56 for Zn, and 0.48 for Re). There are also other trends that are not easily captured by a simple regression line. For example, in a plot of $\delta^{238}U$ vs. TOC, samples with

6.5 wt.% TOC or less produce an R^2 value for a linear regression with $\delta^{238}U$ of 0.91. Above a TOC value of 6.5 wt.%, however, there is no relationship between $\delta^{238}U$ and TOC. A similar pattern is seen for some trace metal concentrations vs. $\delta^{238}U$.

We have several ideas for explaining these trends. Instead of being related directly to bottom-water redox conditions (ferruginous vs. euxinic), $\delta^{238}U$ values show some correlation with TOC and the concentration of transition metals related to productivity such as Ni and Zn. These relationships are stronger in some cores vs. others and are stronger over some ranges of TOC and metal concentrations than others. This supports recent work by Bruggmann et al. (2022) from the modern Peruvian margin and Lau et al. (2022) from Miocene black shales that suggest U can be sorbed onto or incorporated into organic matter in the water column. If isotopically-heavy U(IV) is sorbed onto sinking organic matter in the water column, then a correlation between higher TOC and higher $\delta^{238}U$ values would be expected, which is what we observe in the Sunbury Shale. TOC concentrations would also affect the level of microbially-mediated U reduction, which also drives U isotope fractionation. These relationships could also be related to diffusive input of U to the sediment by U reduction at the sediment-water interface, where other metals such as Mo and V are also subject to the same process. These data also suggest that there was active U reduction in the water column associated with high rates of primary productivity in the Appalachian Basin, driving large degrees of U isotope fractionation such as in the modern Framvaren Fjord, regardless of whether euxinic or ferruginous conditions were present. Ultimately, these data suggest that basin hydrography, productivity, and organic carbon

loading are more important for U isotope fractionation than whether euxinic or ferruginous conditions are present.

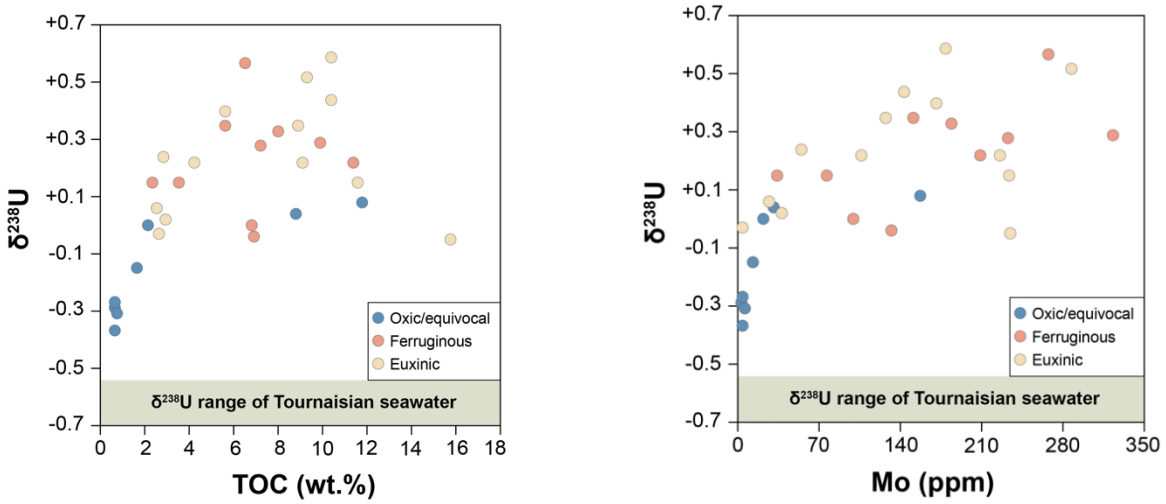

Figure 12. U isotope values vs. TOC and Mo concentrations in samples analyzed from the Sunbury Shale. Samples are color-coded by Fe speciation signal and the U isotope range of Tournaisian seawater comes from the coeval carbonates from Nevada.

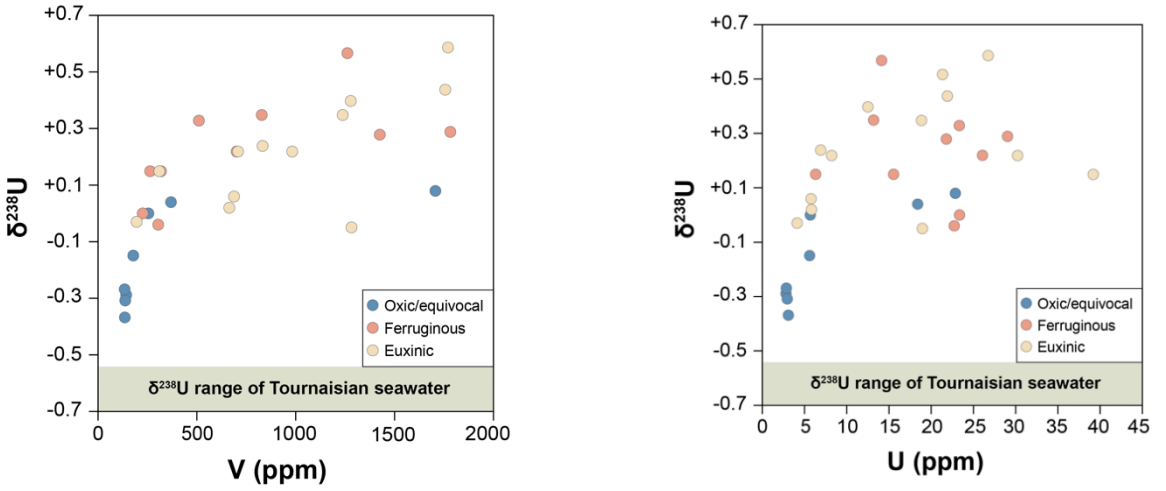

Figure 13. U isotope values vs. V and U concentrations in samples analyzed from the Sunbury Shale. Samples are color-coded by Fe speciation signal and the U isotope range of Tournaisian seawater comes from the coeval carbonates from Nevada.

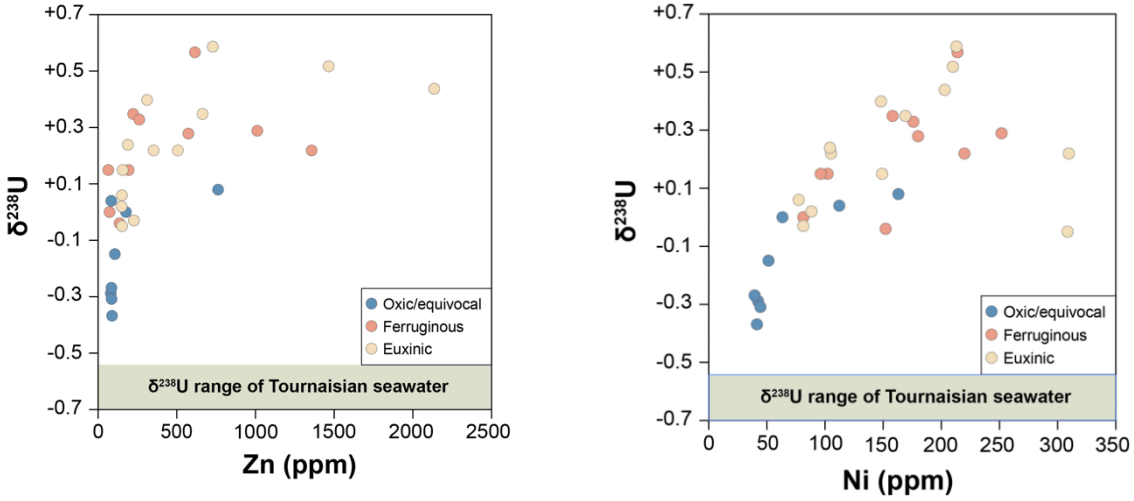

Figure 14. U isotope values vs. Zn and Ni concentrations in samples analyzed from the Sunbury Shale. Samples are color-coded by Fe speciation signal and the U isotope range of Tournaisian seawater comes from the coeval carbonates from Nevada.

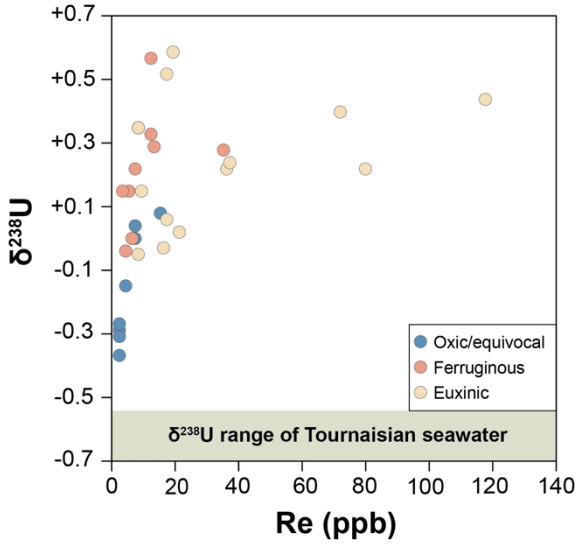

Figure 15. U isotope values vs. Re concentrations in samples analyzed from the Sunbury Shale. Samples are color-coded by Fe speciation signal and the U isotope range of Tournaisian seawater comes from the coeval carbonates from Nevada.

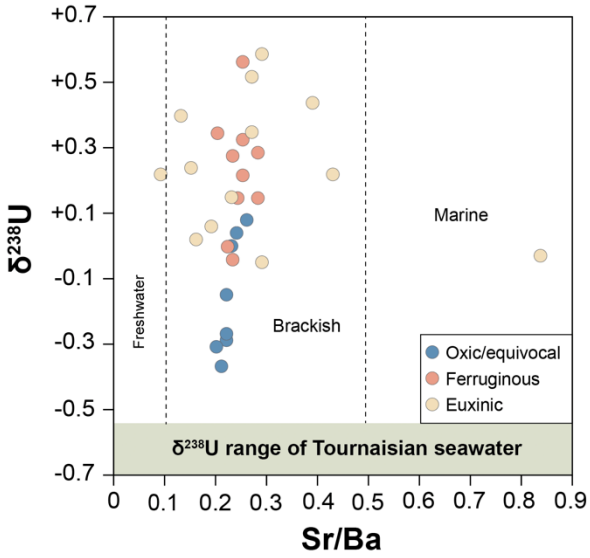

Figure 16. U isotope values vs. Sr/Ba ratios in samples analyzed from the Sunbury Shale (Sr/Ba ratio cutoff values from Wei and Algeo, 2020). Samples are color-coded by Fe speciation signal and the U isotope range of Tournaisian seawater comes from the coeval carbonates from Nevada.

Stratigraphic trends in U isotope through the Sunbury Shale

We also evaluated stratigraphic trends in U isotope data through each of the five study cores and compared them to trends seen in coeval carbonates from Nevada (Cheng et al., 2020). The Nevada carbonate section shows an increasing U isotope trend through the *sanbergi* conodont Zone from approximately −0.40 to −0.25‰ (Fig. 9). The CH and LC cores show the opposite stratigraphic trend, however, with decreasing U isotope values through time (Figs. 16 and 20). In the case of the CH core, this decrease mirrors a progressive decrease in TOC values from 2.1 to 0.6 wt.%. Sr/Ba values remain steady near 0.22, indicating low-brackish conditions. In the case of the CH core, then, we propose a local redox and organic carbon loading control on U isotope values through time, with higher U isotope values associated with more anoxic conditions and higher organic carbon loading, and the shift towards lower U isotope values associated with a shift to more oxic and lower TOC conditions. In the LC core, the progressive decrease in U isotope values through time is mirrored by both a progressive drop in TOC and Sr/Ba. TOC drops from 11.3 to 2.5 wt.% and Sr/Ba drops from a high of 0.83 at the base (indicating marine conditions) to a low of 0.13 towards the top (indicating low-brackish to nearly freshwater conditions). We suggest, then, that U isotope values in the LC core are controlled by local watermass mixing. Gilleaudeau et al. (2021) inferred a shallow mixing zone in the position of the LC core as environments shoaled towards the Cumberland Sill, with frequent changes in redox and salinity. These mixing processes (and a shift towards more ventilated and lower salinity conditions through time) clearly was the primary control on U isotope values in the LC core.

In the DW, RC, and KEP cores, however, there are increasing trends in U isotope values through time (Figs. 17-19), which matches the global seawater trend inferred from the carbonates from Nevada (Cheng et al., 2020). In these cores, TOC and Sr/Ba values are more constant through time, suggesting that there was more persistent anoxia and a lack of changes in salinity in these deep-water environments, potentially implying that a global redox signal is being preserved in these cores. However, the magnitude of shift in U isotopes is much higher in the DW, RC, and KEP cores compared with seawater inferred from carbonates in Nevada, suggesting that there is still a strong local control on U isotope values in the Sunbury Shale.

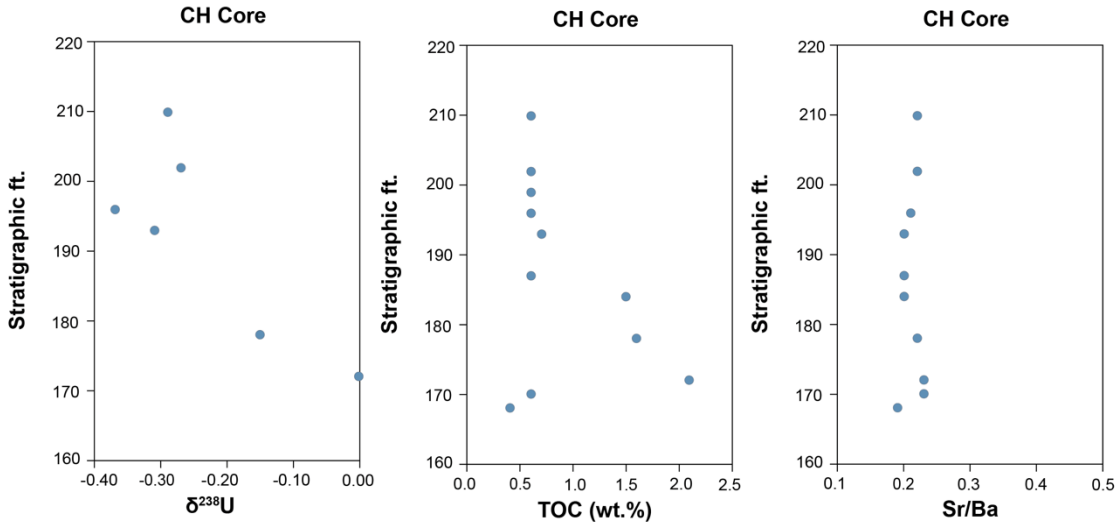

Figure 17. Stratigraphic trends in U isotopes, TOC, and Sr/Ba ratios in the CH core (northeastern Ohio).

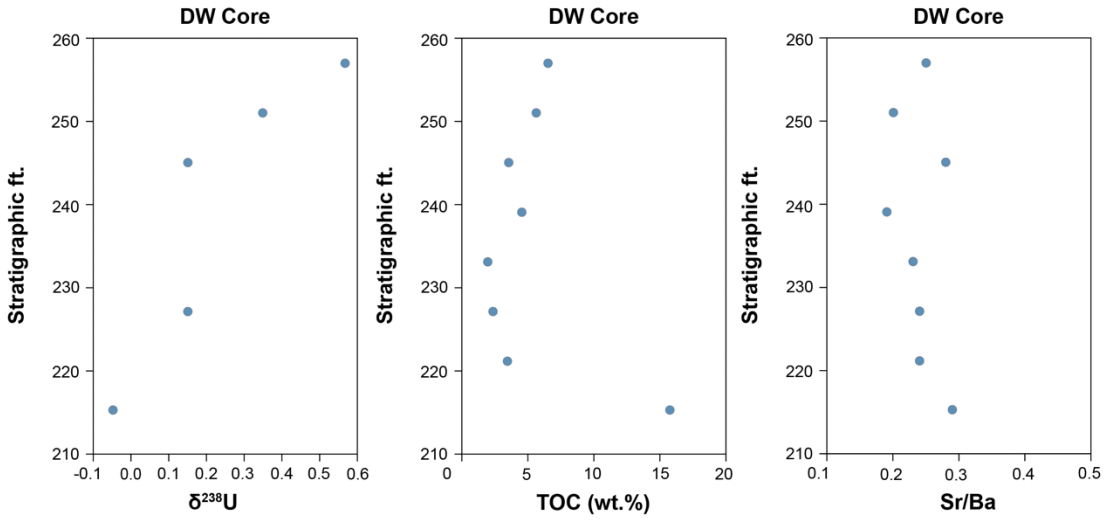

Figure 18. Stratigraphic trends in U isotopes, TOC, and Sr/Ba ratios in the DW core (central Ohio).

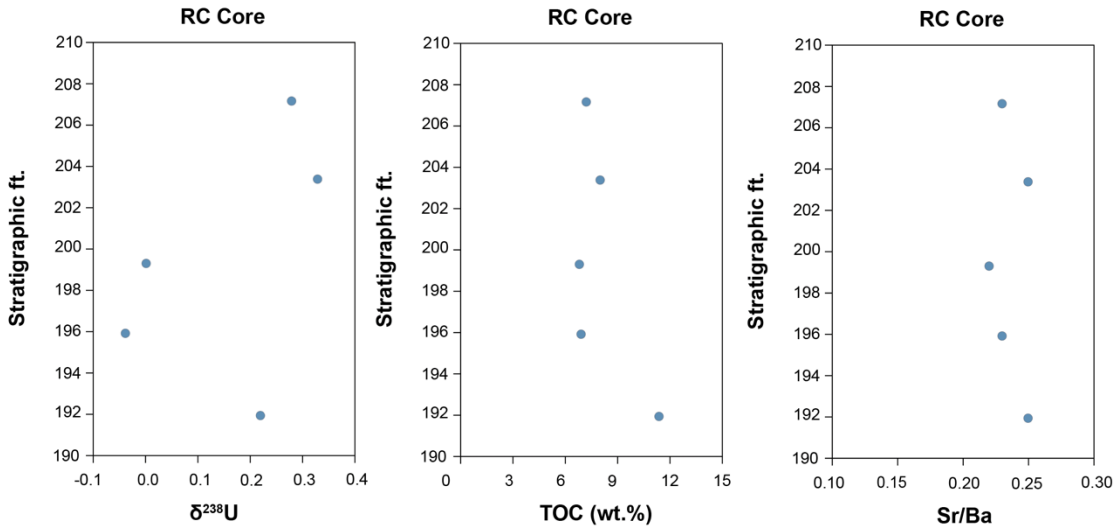

Figure 19. Stratigraphic trends in U isotopes, TOC, and Sr/Ba ratios in the RC core (south-central Ohio).

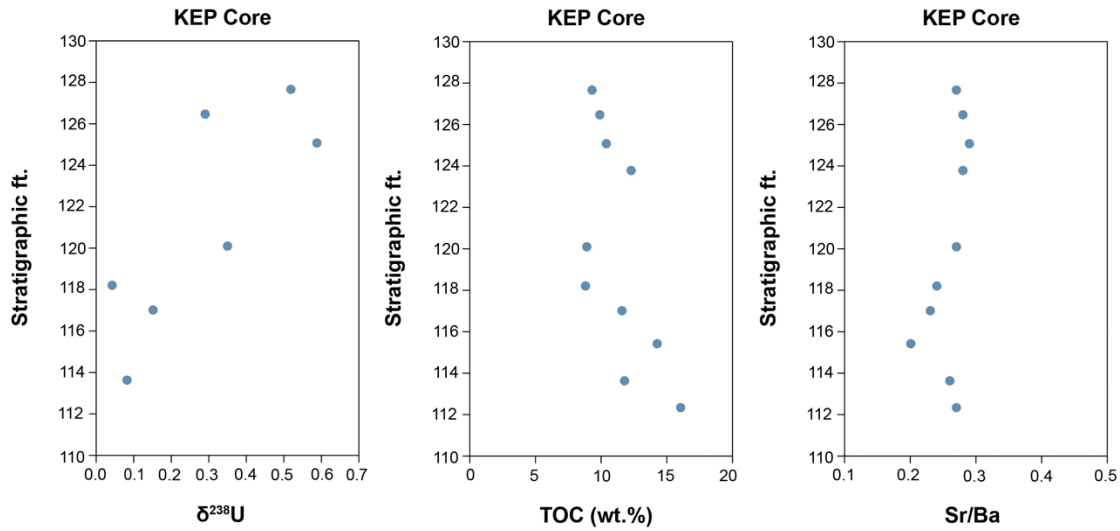

Figure 20. Stratigraphic trends in U isotopes, TOC, and Sr/Ba ratios in the KEP core (central Kentucky).

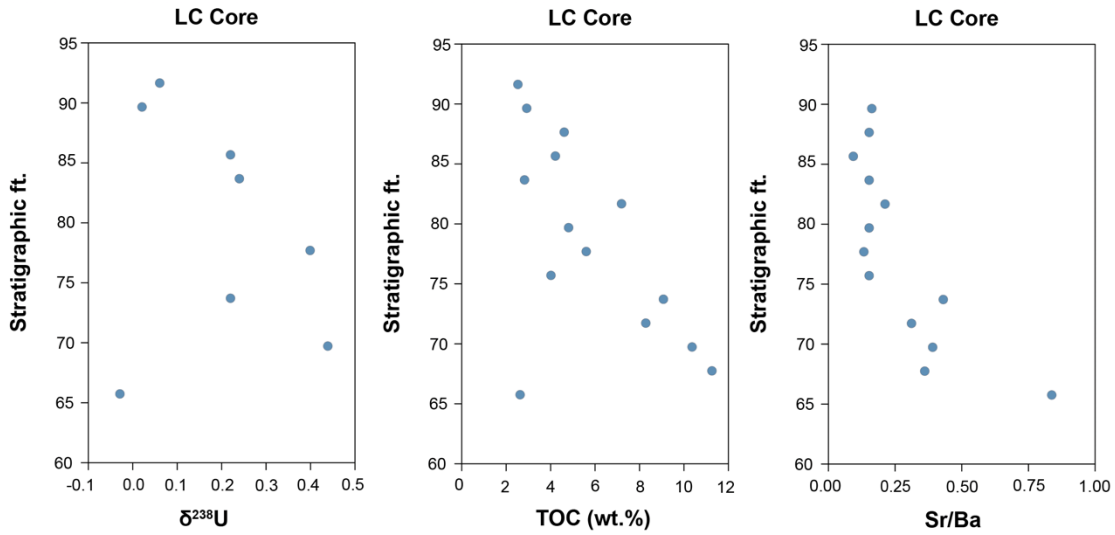

Figure 21. Stratigraphic trends in U isotopes, TOC, and Sr/Ba ratios in the LC core (southern Kentucky).

Evaluation of hypotheses

These data suggest that our main hypothesis is falsified, with no relationship observed between iron speciation and $\delta^{238}U$ for anoxic samples. Instead, our data support our alternative hypothesis, suggesting that local factors other than bottom-water redox, such as primary productivity and organic carbon loading are more important for determining the degree of U isotope fractionation during U removal to reducing sediments. This is similar to conclusions drawn from the modern Peruvian upwelling zone (Bruggmann et al., 2022) and the Miocene Monterey Formation (Lau et al., 2022). Local controls are also more apparent in some cores than others, with this effect highly dependent on basin hydrography and watermass mixing.

Implications for the U isotope paleo-redox proxy

Overall, these results necessitate a reassessment of the processes that control the $\delta^{238}U$ composition of seawater over geologic time. Clearly, the global extent of anoxia exerts a strong control on the $\delta^{238}U$ composition of seawater, but other factors need to be considered such as primary productivity and organic carbon loading. For example, strong pulses of eutrophication in the oceans could drive strong removal of isotopically-heavy U(IV) to sediments, driving the $\delta^{238}U$ value of seawater to lower values. This could happen regardless of whether expanded anoxia was accompanied by ferruginous or euxinic conditions. This could partly explain the shift towards lower carbonate $\delta^{238}U$ values across the Late Devonian mass extinctions (White et al., 2018; Zhang et al., 2020), the Permo-Triassic extinction (see Zhang et al., 2018 for review), and Cretaceous OAE 2 (Clarkson et al., 2018; Kulenguski et al., in review). While these events are known to be associated with expanded marine anoxia, enhanced nutrient delivery and eutrophication of the oceans could drive large degrees of U isotope fractionation even if only small amounts of the global seafloor became anoxic. In contrast, carbonate $\delta^{238}U$ values close to modern seawater through a large interval of the mid-Proterozoic is difficult to explain given that mid-Proterozoic oceans are generally assumed to have been largely anoxic (Gilleaudeau et al., 2019). Gilleaudeau et al. (2019) hypothesized that this was related to a general lack of euxinia in the mid-Proterozoic oceans, with the persistence of ferruginous deep oceans leading to minimal degrees of U isotope fractionation. This study suggests, however, that

low rates of primary productivity in the mid-Proterozoic oceans could explain the lack of U isotope fractionation, thus leading to carbonate $\delta^{238}U$ values close to modern seawater. Many recent studies have suggested a substantially less productive biosphere during the Proterozoic compared to today (Crockford et al., 2018; Laakso et al., 2019). This study does not nullify the general idea that the degree of marine anoxia exerts a strong control on the $\delta^{238}U$ values of seawater; however, it does suggest that changes in the abundance of highly productive continental margins, restricted basins, or epeiric seas in the geologic past could drive large changes in the $\delta^{238}U$ composition of seawater through time, regardless of whether completely euxinic or ferruginous conditions were reached on the seafloor. This could complicate any quantitative approaches for determining the extent of anoxic seafloor based on carbonate $\delta^{238}U$ data.

This study also has important implications for using black shales as an archive for the U isotope composition of seawater through geologic time. Whereas most recent studies recognize the importance of local processes controlling the U isotope composition of black shales, several studies have attempted to use a constant offset between anoxic sediments and seawater to reconstruct seawater U isotope values. Montoya-Pino et al. (2010) estimated the degree of ocean anoxia during Cretaceous OAE 2 using black shale U isotopes and Kendall et al. (2015) inferred a major Ediacaran ocean oxygenation episode also using U isotopes in black shales. In contrast, Kendall et al. (2020) recognized local controls on the U isotope composition of black shales from the Devonian Kettle Point Formation, Canada.

Our study suggests that U isotope values and trends can be drastically different through black shale profiles through the same time interval and in the same basin on the scale of 100s of km or less. As discussed earlier, both the CH and LC cores show the opposite stratigraphic trend compared to global seawater inferred using carbonate U isotope values in Nevada (Cheng et al., 2020). This is because of strong local controls related to organic carbon loading and salinity, which are ultimately related to basin hydrography and watermass mixing. The DW, RC, and KEP cores show a stratigraphic trend that more closely resembles the seawater trend inferred from coeval carbonates, likely because these cores were deposited in more persistently anoxic deeper-water environments less prone to local controls. Interestingly, the offset between U isotope values in the DW, RC, and KEP cores and our estimate of coeval seawater is ~0.6 to 0.8‰, which is similar to the offset assumed when reconstructing seawater U isotope values from black shales in studies such as Montoya-Pino et al. (2010) and Kendall et al. (2015). This suggests there is some validity to these methods; however, without the coeval carbonate data, it would be difficult to determine which of the Sunbury Shale cores to trust if attempting to reconstruct seawater U isotope values. We suggest that instead of focusing on whether samples were deposited under euxinic or ferruginous conditions, future studies should use a range of proxies to test for the persistence of anoxia, uniform organic carbon loading, and uniformly brackish or marine salinities in deciding which black shales might best be used to reconstruct seawater U isotope values.

CONCLUSIONS

The main goal of this project was to further understand the U isotope proxy and what drives the fractionation of $^{238}U/^{235}U$ in a variety of redox environments. Evolution and extinction of life on Earth is closely tied to the abundance of oxygen in the atmosphere-ocean system. While the U isotope proxy has been useful in determining the extent of global ocean anoxia in the geologic past, it is less clear how fractionation differs under ferruginous vs. euxinic conditions, with ferruginous conditions more abundant earlier in Earth history. The North American intracratonic basins of the Late Devonian-Early Mississippian provide an excellent environment to test this proxy because sediments were deposited coevally under a variety of redox conditions over relatively short spatial distances. Five cores of the Lower Mississippian (Tournaisian) Sunbury Shale were taken along a transect of the Appalachian Basin from the Catskill Delta in the northeast to the Cumberland Sill in the southwest. Based on iron speciation data, these five cores were determined to be deposited across a redoxcline of coeval oxic, ferruginous, and euxinic conditions. When considering all five cores, oxic to equivocal samples based on iron speciation showed U isotope values ranging from −0.37 to +0.08‰, whereas ferruginous samples ranged from −0.04 to +0.57‰, and euxinic samples from −0.05 to +0.59‰. These data suggests that U isotopes can be strongly fractionated during U(VI) to U(IV) reduction in both euxinic and ferruginous environments.

$\delta^{238}U$ values from the five Sunbury Shale cores were also compared to carbonates from Nevada deposited coevally in the *sanbergi* conodont Zone. Global oceans during this

time had a $\delta^{238}U$ composition between −0.70 to −0.55‰, suggesting more expanded global anoxia compared to today. We used these inferred Tournaisian seawater compositions to calculate $\Delta^{238}U$ values ($\delta^{238}U_{sample} - \delta^{238}U_{seawater}$). In oxic to equivocal samples based on iron speciation, $\Delta^{238}U$ values range from 0.18 to 0.70‰. $\Delta^{238}U$ values of ferruginous samples range from 0.51 to 1.27‰ and euxinic sample $\Delta^{238}U$ values range from 0.50 to 1.29‰. $\delta^{238}U$ values were also compared to TOC and redox sensitive trace metals. In some cores, $\delta^{238}U$ values showed a strong correlation with TOC and trace metals sensitive to productivity, whereas others showed little correlation. Increasing U isotope values over time in the DW, RC, and KEP cores mirror those in global seawater based on the carbonates from Nevada. However, U isotope values in the CH and LC cores show a decreasing trend stratigraphically, suggesting completely local controls on U isotope values.

The findings in this study shed new light on the mechanisms that control U isotope fractionation. The reduction of U(VI) to U(IV) in euxinic and ferruginous redox environments removes ^{238}U from the water column and transfers it to the sediments, leaving lower $\delta^{238}U$ in the water column and higher $\delta^{238}U$ in sediments. Samples taken from cores with persistently anoxic conditions below the redoxcline and under stable brackish salinities show strong and somewhat consistent U isotope fractionation from seawater. An increase in U isotope values over time in these cores loosely mirrors global seawater trends as inferred from the Nevada carbonates. Samples taken from cores with fluctuating redox conditions and either low or variable salinities indicating frequent watermass mixing show more variable U isotope values that are entirely controlled by local processes. Ultimately, we find that the main controls on U isotope fractionation in both

euxinic and ferruginous environments are organic carbon loading, productivity, and basin hydrography. Samples with high TOC show strong U isotope fractionation, as in the modern Peruvian upwelling zone and the Miocene Monterey Formation. Isotopically-heavy, reduced U(IV) is incorporated into raining organic matter in the water column, enriching sediments in ^{238}U. High productivity and organic carbon loading also increases the degree of microbially-mediated U reduction in the water column, as is seen in the modern Framvaren Fjord. Samples deposited near riverine influx from the Catskill Delta and samples located close to a shallow mixing zone over the Cumberland Sill showed a lower and more variable degree of U isotope fraction. Basin hydrography and the degree of basin mixing with the global ocean system are a major control on the degree of U isotope fractionation. This study provides important new information that should be considered when interpreting U isotope values from the geologic record.

ADDITIONAL TABLES

Table 1. Sample information along with TC (total carbon), TS (total sulfur), TOC (total organic carbon), NAVS (non-acid-volatile sulfur), TIC (total inorganic carbon), and AVS (acid-volatile sulfur) data for all samples in this study.

Sample	Strat Feet	TC (wt.%)	TS (wt.%)	TOC (wt.%)	NAVS (wt.%)	TIC (wt.%)	AVS (wt.%)
CH-60	210.0	0.4	1.3	0.6	1.0	0.0	0.3
CH-68	202.0	0.5	1.2	0.6	0.8	0.0	0.4
CH-74	196.0	0.5	1.4	0.6	0.9	0.0	0.4
CH-77	193.0	0.5	1.4	0.7	1.1	0.0	0.3
CH-92	178.0	0.8	1.9	1.6	1.5	0.0	0.3
CH-98	172.0	1.9	1.3	2.1	1.0	0.0	0.3
DW-112.7	227.1	2.3	2.0	2.3	0.9	0.0	1.1
DW-124.6	215.2	15.8	10.2	15.8	8.8	0.1	1.4
DW-82.7	257.1	6.9	2.2	6.5	1.2	0.4	0.9
DW-88.7	251.1	5.6	1.8	5.6	1.0	0.0	0.8
DW-94.7	245.1	3.5	2.3	3.5	0.9	0.0	1.5
KEP -3-52.5	127.7	9.3	2.6	9.3	1.6	0.0	1.0
KEP -3-53.7	126.5	9.9	4.0	9.9	2.6	0.1	1.4
KEP -3-55.1	125.1	10.4	2.9	10.4	2.0	0.0	0.8
KEP -3-60.1	120.1	8.9	2.6	8.9	1.7	0.0	0.9
KEP -3-62.0	118.2	8.8	1.6	8.8	1.1	0.0	0.5
KEP -3-63.2	117	11.6	2.6	11.6	1.7	0.0	0.8
KEP -3-66.6	113.6	11.8	1.8	11.8	1.3	0.0	0.5
LC -2683.5	91.7	2.5	2.1	2.5	1.6	0.0	0.5

LC - 2685.5	89.7	2.9	2.6	2.9	2.4	0.0	0.2
LC - 2689.5	85.7	4.2	2.2	4.2	2.0	0.0	0.2
LC - 2691.5	83.7	3.0	2.6	2.8	2.3	0.2	0.4
LC - 2697.5	77.7	5.6	1.9	5.6	1.6	0.0	0.3
LC - 2701.5	73.7	9.1	5.7	9.1	5.8	0.0	0.0
LC - 2705.5	69.7	10.6	1.8	10.4	1.3	0.2	0.5
LC - 2709.5	65.7	4.0	4.4	2.6	3.2	1.5	1.2
RC-103.6	191.9	11.4	2.9	11.4	2.3	0.0	0.6
RC-88.3	207.2	7.2	2.3	7.2	1.8	0.0	0.5
RC-92.1	203.4	8.0	2.4	8.0	1.6	0.0	0.8
RC-96.2	199.3	6.8	1.9	6.8	1.4	0.0	0.5
RC-99.6	195.9	6.9	1.8	6.9	1.4	0.0	0.4

Table 2. Sample information along with Al, P, Ti, V, Cr, Mn, Fe, and Ni concentration data for all samples in this study.

Sample	Strat feet	Al (wt.%)	P (ppm)	Ti (ppm)	V (ppm)	Cr (ppm)	Mn (ppm)	Fe (wt.%)	Ni (ppm)
CH-60	210.0	8.26	254	4781	137	88	147	3.93	42
CH-68	202.0	7.94	227	4847	129	85	146	3.78	39
CH-74	196.0	8.13	206	5086	130	89	152	3.94	41
CH-77	193.0	8.17	195	4735	132	85	148	3.90	44
CH-92	178.0	10.81	321	5520	173	110	200	5.56	51
CH-98	172.0	8.36	321	4463	250	91	140	3.77	63
DW-112.7	227.1	7.74	180	3546	314	78	112	3.71	96
DW-124.6	215.2	4.35	498	3021	1284	109	86	9.67	309
DW-82.7	257.1	5.77	236	3600	1263	106	125	3.80	214
DW-88.7	251.1	4.17	224	3758	827	94	107	3.41	158
DW-94.7	245.1	7.34	185	3511	259	77	113	3.95	102
KEP -3-52.5	127.7	7.47	207	3179	2106	132	133	3.95	210
KEP -3-53.7	126.5	6.68	246	2896	1787	100	91	4.89	252
KEP -3-55.1	125.1	6.68	267	3216	1775	108	101	4.08	213
KEP -3-60.1	120.1	6.48	240	3209	1239	90	100	3.69	169
KEP -3-62.0	118.2	6.06	256	2975	365	101	88	2.88	112
KEP -3-63.2	117	5.82	259	2772	306	61	109	3.20	149
KEP -3-66.6	113.6	6.24	324	3287	1711	113	102	3.23	163
LC -2683.5	91.7	8.43	201	4004	686	107	112	4.00	77
LC -2685.5	89.7	8.57	188	4033	662	104	115	4.31	88
LC -2689.5	85.7	7.33	187	4037	982	105	99	3.48	105
LC -2691.5	83.7	8.14	188	3922	831	100	103	4.06	104

LC - 2697.5	77.7	6.77	188	3489	1280	95	106	2.97	148
LC - 2701.5	73.7	5.15	329	2672	706	82	102	5.93	310
LC - 2705.5	69.7	5.50	496	3235	1761	103	95	2.34	203
LC - 2709.5	65.7	5.22	749	4372	190	75	227	4.91	81
RC-103.6	191.9	7.05	309	3520	699	84	142	4.20	220
RC-88.3	207.2	6.73	198	3126	1428	95	107	3.80	180
RC-92.1	203.4	4.24	277	3330	507	75	115	3.64	176
RC-96.2	199.3	7.84	241	3746	221	80	147	3.96	81
RC-99.6	195.9	6.98	194	3397	300	74	137	3.44	152

Table 3. Sample information along with Cu, Zn, Sr, Mo, Ba, Re, and U concentration data for all samples in this study.

Sample	Strat feet	Cu (ppm)	Zn (ppm)	Sr (ppm)	Mo (ppm)	Ba (ppm)	Re (ppb)	U (ppm)
CH-60	210.0	20	73	74	2	342	2	2.73
CH-68	202.0	19	77	75	3	334	2	2.77
CH-74	196.0	21	81	73	3	345	2	3.01
CH-77	193.0	23	78	70	5	344	2	2.88
CH-92	178.0	36	99	100	12	460	4	5.54
CH-98	172.0	28	170	78	21	347	7	5.62
DW-112.7	227.1	35	187	90	33	383	3	6.27
DW-124.6	215.2		145	62	235	214	8	18.93
DW-82.7	257.1		611	83	268	324	12	14.10
DW-88.7	251.1		216	56	151	281	8	13.15
DW-94.7	245.1	35	57	97	76	343	5	15.52
KEP -3-52.5	127.7	74	1466	114	288	417	17	21.34
KEP -3-53.7	126.5	89	1010	104	324	377	13	29.06
KEP -3-55.1	125.1	91	725	105	179	359	19	26.77
KEP -3-60.1	120.1	67	660	106	127	399	8	18.83
KEP -3-62.0	118.2	74	76	100	30	422	7	18.38
KEP -3-63.2	117	60	149	92	234	406	9	39.29
KEP -3-66.6	113.6	109	759	98	157	379	15	22.86
LC -2683.5	91.7	52	144	75	26	400	17	5.67
LC -2685.5	89.7	53	142	78	37	500	21	5.72
LC -2689.5	85.7	54	347	69	106	738	36	8.12
LC -2691.5	83.7	58	182	79	54	524	37	6.82
LC -2697.5	77.7	57	305	70	171	534	72	12.44
LC -2701.5	73.7	90	502	136	226	316	80	30.28

LC - 2705.5	69.7	106	2141	122	143	311	118	21.91
LC - 2709.5	65.7	68	221	534	3	638	16	4.01
RC-103.6	191.9	82	1357	83	209	331	7	26.08
RC-88.3	207.2	70	569	80	233	353	35	21.79
RC-92.1	203.4	60	255	60	184	246	12	23.33
RC-96.2	199.3	47	65	80	99	365	6	23.36
RC-99.6	195.9	49	129	77	132	331	4	22.73

Table 4. Sample information along with Fe-py (pyrite Fe), Fe-carb (carbonate Fe), Fe-ox (oxide Fe), Fe-mag (magnetite Fe), Fe-HR (highly reactive Fe), Fe-HR/T (highly reactive Fe/total Fe), Fe-py/HR (pyrite Fe/highly reactive Fe), and δ^{34}S-py (pyrite sulfur isotope) data for all samples in this study.

Sample	Strat feet	Fe-py (wt.%)	Fe-carb (wt.%)	Fe-ox (wt.%)	Fe-mag (wt.%)	Fe-HR (wt.%)	Fe-HR/T	Fe-py/HR	δ^{34}S-py (‰ vs. VCDT)
CH-60	210.0	0.69	0.12	0.43	0.16	1.40	0.36	0.49	-27.4
CH-68	202.0	0.66	0.17	0.44	0.14	1.41	0.37	0.47	-28.0
CH-74	196.0	0.47	0.00	0.54	0.17	1.17	0.30	0.40	-30.3
CH-77	193.0		0.14	0.39	0.20				
CH-92	178.0	1.16	0.13	0.31	0.13	1.73	0.31	0.67	-23.6
CH-98	172.0	0.67	0.20	0.17	0.11	1.14	0.30	0.59	-27.4
DW-112.7	227.1	1.09	0.01	0.37	0.45	1.91	0.52	0.57	-24.1
DW-124.6	215.2	7.49	0.39	0.90	0.14	8.93	0.92	0.84	-8.1
DW-82.7	257.1	1.14	0.06	0.25	0.41	1.86	0.49	0.62	-30.5
DW-88.7	251.1	1.04	0.05	0.29	0.30	1.68	0.49	0.62	-26.0
DW-94.7	245.1	1.08	0.02	0.49	0.70	2.29	0.58	0.47	-27.9
KEP-3-52.5	127.7	1.44	0.04	0.02	0.19	1.69	0.43	0.85	-34.4
KEP-3-53.7	126.5	1.93	0.09	0.03	0.55	2.60	0.53	0.74	-34.3
KEP-3-55.1	125.1	1.34	0.05	0.03	0.22	1.63	0.40	0.82	-33.7
KEP-3-60.1	120.1	1.40	0.04	0.02	0.13	1.59	0.43	0.88	-31.0

KEP-3-62.0	118.2	0.70	0.03	0.02	0.12	0.87	0.30	0.81	-33.3
KEP-3-63.2	117	1.30	0.04	0.02	0.16	1.51	0.47	0.86	-28.6
KEP-3-66.6	113.6	0.93	0.05	0.02	0.09	1.08	0.34	0.86	-23.8
LC-2683.5	91.7	1.70	0.07	0.10	0.11	1.97	0.49	0.86	-21.1
LC-2685.5	89.7	2.13	0.08	0.08	0.11	2.40	0.56	0.89	-18.4
LC-2689.5	85.7	1.64	0.09	0.04	0.06	1.83	0.53	0.90	-27.1
LC-2691.5	83.7	2.17	0.09	0.05	0.06	2.36	0.58	0.92	-20.7
LC-2697.5	77.7	1.18	0.12	0.05	0.02	1.38	0.46	0.86	-27.3
LC-2701.5	73.7		0.16	0.18	0.04				
LC-2705.5	69.7	1.08	0.11	0.06	0.02	1.28	0.55	0.85	-12.0
LC-2709.5	65.7	3.40	0.26	0.08	0.04	3.78	0.77	0.90	-9.0
RC-103.6	191.9	1.84	0.11	0.27	0.32	2.55	0.61	0.72	-18.7
RC-88.3	207.2	1.53	0.07	0.22	0.22	2.04	0.54	0.75	-36.1
RC-92.1	203.4	1.41	0.06	0.42	0.41	2.30	0.63	0.61	-29.9
RC-96.2	199.3	1.11	0.06	0.38	0.38	1.93	0.49	0.58	-23.1
RC-99.6	195.9	1.13	0.08	0.29	0.26	1.77	0.52	0.64	-22.1

Table 5. Sample information along with $\delta^{238}U$, 2 sd of replicate measurements, n (number of measurements), and Sr/Ba data for all samples in this study.

Sample	Strat feet	$\delta^{238}U$	2 sd	n	Sr/Ba
CH-60	210.0	-0.29	0.05	2	0.22
CH-68	202.0	-0.27	0.06	2	0.22
CH-74	196.0	-0.37	0.08	2	0.21
CH-77	193.0	-0.31	0.05	2	0.20
CH-92	178.0	-0.15	0.01	2	0.22
CH-98	172.0	0.00	0.03	2	0.23
DW-112.7	227.1	0.15	0.03	2	0.24
DW-124.6	215.2	-0.05	0.10	3	0.29
DW-82.7	257.1	0.57	0.13	3	0.25
DW-88.7	251.1	0.35	0.04	3	0.20
DW-94.7	245.1	0.15	0.15	3	0.28
KEP -3- 52.5	127.7	0.52	0.03	3	0.27
KEP -3- 53.7	126.5	0.29	0.03	2	0.28
KEP -3- 55.1	125.1	0.59	0.07	2	0.29
KEP -3- 60.1	120.1	0.35	0.05	2	0.27
KEP -3- 62.0	118.2	0.04	0.06	2	0.24
KEP -3- 63.2	117	0.15	0.10	2	0.23
KEP -3- 66.6	113.6	0.08	0.00	2	0.26
LC - 2683.5	91.7	0.06	0.02	2	0.19
LC - 2685.5	89.7	0.02	0.11	2	0.16
LC - 2689.5	85.7	0.22	0.10	2	0.09
LC - 2691.5	83.7	0.24	0.12	2	0.15
LC - 2697.5	77.7	0.40	0.03	2	0.13
LC - 2701.5	73.7	0.22	0.09	2	0.43
LC - 2705.5	69.7	0.44	0.10	2	0.39
LC - 2709.5	65.7	-0.03	0.05	2	0.84
RC-103.6	191.9	0.22	0.06	2	0.25
RC-88.3	207.2	0.28	0.07	2	0.23
RC-92.1	203.4	0.33	0.12	2	0.25
RC-96.2	199.3	0.00	0.12	2	0.22
RC-99.6	195.9	-0.04	0.01		0.23

REFERENCES

Adelson, J. M., Helz, G. R., & Miller, C. V. (2001). Reconstructing the rise of recent coastal anoxia; molybdenum in Chesapeake Bay sediments. *Geochimica et Cosmochimica Acta*, *65*(2), 237–252. https://doi.org/10.1016/S0016-7037(00)00539-1.

Algeo, T.J., Scheckler, S.E. (1998). Terrestrial-marine teleconnections in the Devonian: Links between the evolution of land plants, weathering processes, and marine anoxic events. *Philosophical Transactions of the Royal Society of London. Series B: Biological Sciences*, *353*, 113–130: https://doi.org/10.1098/rstb.1998.0195.

Algeo, T.J., Woods, A.D. (1994). Microstratigraphy of the Lower Mississippian Sunbury Shale: A record of solar-modulated climatic cyclicity. *Geology*, *22*, 795: https://doi.org/10.1130/0091-7613(1994)022<0795:MOTLMS>2.3.CO;2.

Andersen, M.B., Romaniello, S.J, Vance, D., Little, S.H., Herdman, R., Lyons, T.W. (2014). A modern framework for the interpretation of $^{238}U/^{235}U$ in studies of ancient ocean redox. *Earth and Planetary Science Letters*, *400*, 184–194: https://doi.org/10.1016/j.epsl.2014.05.051.

Bianchi, T. S., DiMarco, S. F., Cowan, J. H., Hetland, R. D., Chapman, P., Day, J. W., & Allison, M. A. (2010). The science of hypoxia in the Northern Gulf of Mexico: A review. *Science of The Total Environment*, *408*(7), 1471–1484. https://doi.org/10.1016/j.scitotenv.2009.11.047.

Bowyer, F. T., Shore, A. J., Wood, R. A., Alcott, L. J., Thomas, A. L., Butler, I. B., Curtis, A., Hainanan, S., Curtis-Walcott, S., Penny, A. M., & Poulton, S. W. (2020). Regional nutrient decrease drove redox stabilisation and metazoan diversification in the late Ediacaran Nama Group, Namibia. *Scientific Reports*, *10*(1), 2240. https://doi.org/10.1038/s41598-020-59335-2.

Brennecka, G.A., Herrmann, A.D., Algeo, T.J., Anbar, A.D. (2011). Rapid expansion of oceanic anoxia immediately before the end-Permian mass extinction. *Proceedings of the National Academy of Sciences*, *108*(43), 17631–17634. https://doi.org/10.1073/pnas.1106039108

Brezinski, D.K., Cecil, C.B., Skema, V.W., Stamm, R. (2008). Late Devonian glacial deposits from the eastern United States signal an end of the mid-Paleozoic warm period. *Palaeogeography, Palaeoclimatology, Palaeoecology*, *268*(3–4), 143–151. https://doi.org/10.1016/j.palaeo.2008.03.042

Chen, X., Romaniello, S. J., Herrmann, A. D., Hardisty, D., Gill, B. C., & Anbar, A. D. (2018). Diagenetic effects on uranium isotope fractionation in carbonate sediments from the Bahamas. *Geochimica et Cosmochimica Acta*, *237*, 294–311. https://doi.org/10.1016/j.gca.2018.06.026

Cheng, K., Elrick, M., & Romaniello, S. J. (2020). Early Mississippian ocean anoxia triggered organic carbon burial and late Paleozoic cooling: Evidence from uranium isotopes recorded in marine limestone. *Geology*, *48*(4), 363–367. https://doi.org/10.1130/G46950.1

Clarkson, M. O., Stirling, C. H., Jenkyns, H. C., Dickson, A. J., Porcelli, D., Moy, C. M., Pogge von Strandmann, P. A. E., Cooke, I. R., & Lenton, T. M. (2018). Uranium isotope evidence for two episodes of deoxygenation during Oceanic Anoxic Event 2. *Proceedings of the National Academy of Sciences*, *115*(12), 2918–2923. https://doi.org/10.1073/pnas.1715278115

Cole, D.B., Planavsky, N.J., Longley, M., Böning, P., Wilkes, D., Wang, X., Swanner, E.D., Wittkop, C., Loydell, D.K., Busigny,V., Knudsen, A.C., Sperling, E.A. (2020). Uranium isotope fractionation in non-sulfidic anoxic settings and the global uranium isotope mass balance. *Global Biogeochemical Cycles*, *34*: https://doi.org/10.1029/2020GB006649.

Comer, J. B. (1991). *Stratigraphic analysis of the upper Devonian Woodford formation, Permian basin, west Texas and southeastern New Mexico* (Vol. 201). USA: Bureau of Economic Geology, University of Texas at Austin.

Crockford, P. W., Hayles, J. A., Bao, H., Planavsky, N. J., Bekker, A., Fralick, P. W., Halverson, G. P., Bui, T. H., Peng, Y., & Wing, B. A. (2018). Triple oxygen isotope evidence for limited mid-Proterozoic primary productivity. *Nature*, *559*(7715), 613–616. https://doi.org/10.1038/s41586-018-0349-y

Egenhoff, S.O., Fishman, N.S. (2020). The Bakken Formation—Understanding the sequence stratigraphic record of low-gradient sedimentary systems, shale depositional environments, and sea-level changes in an icehouse world. *The Sedimentary Record*, *18*(4), 4–9. https://doi.org/10.2110/sedred.2020.4.4.

Ekblaw, G. E. (1938). Kankakee arch in Illinois. *Bulletin of the Geological Society of America*, *49*(9), 1425-1430.

Ettensohn, F.R. (1985). The Catskill Delta complex and the Acadian Orogeny: A model. *In* Geological Society of America Special Paper 201, 39-50.

Faill, R.T. (1997). A geologic history of the north-central Appalachians; Part 1, Orogenesis from the Mesoproterozoic through the Taconic Orogeny. *American Journal of Science*, 297, 551-619: https://doi.org/10.2475/ajs.297.6.551.

Gilleaudeau, G.J., Romaniello, S.J., Luo, G., Kaufman, A.J., Zhang, F., Klaebe, R.M., Kah, L.C., Azmy, K., Bartley, J.K., Zheng, W., Knoll, A.H., Anbar, A.D. (2019). Uranium isotope evidence for limited euxinia in mid-Proterozoic oceans. *Earth and Planetary Science Letters*, *521*, 150–157: https://doi.org/10.1016/j.epsl.2019.06.012.

Gilleaudeau, G.J., Algeo, T.J., Lyons, T.W., Bates, S., Anbar, A.D. (2021). Novel watermass reconstruction in the Early Mississippian Appalachian Seaway based on integrated proxy records of redox and salinity. *Earth and Planetary Science Letters*, *558*, 116746. https://doi.org/10.1016/j.epsl.2021.116746.

Gilleaudeau, G.J., Chen, X., Romaniello, S.J., Wittkop, C., Anbar, A.D., Swanner, E.D. (in preparation). Uranium isotope cycling in ferruginous Canyon Lake, Michigan, USA. *Geochimica et Cosmochimica Acta*.

Gradstein, F.M., Ogg, J.G., Schmitz, M., Ogg, G. (2020). Geologic Time Scale 2020.

Hatcher, R.D. (2010). The Appalachian orogen: A brief summary. *In* Geological Society of America Memoir 206, 1-20.

Helly, J. J., & Levin, L. A. (2004). Global distribution of naturally occurring marine hypoxia on continental margins. *Deep Sea Research Part I: Oceanographic Research Papers*, *51*(9), 1159–1168. https://doi.org/10.1016/j.dsr.2004.03.009

Hemmesch, N.T., Harris, N.B., Mnich, C.A., Selby, D. (2014). A sequence-stratigraphic framework for the Upper Devonian Woodford Shale, Permian Basin, west Texas. *AAPG Bulletin* 98, 23-47.

Hogancamp, N.J., Pocknall, D.T. (2018). The biostratigraphy of the Bakken Formation: A review and new data. *Stratigraphy*, *15*(3), 197–224: https://doi.org/10.29041/strat.15.3.197-224.

Holmden, C., Amini, M., Francois, R. (2015). Uranium isotope fractionation in Saanich Inlet: A modern analog study of a paleoredox tracer. *Geochimica et Cosmochimica Acta, 153*: https://doi.org/10.1016/j.gca.2014.11.012.

Isaacson, P.E., Díaz-Martínez, E., Grader, G.W., Kalvoda, J., Babek, O., Devuyst, F.X. (2008). Late Devonian–earliest Mississippian glaciation in Gondwanaland and its biogeographic consequences. *Palaeogeography, Palaeoclimatology, Palaeoecology*, *268*(3–4), 126–142. https://doi.org/10.1016/j.palaeo.2008.03.047

Jenkyns, H. C. (2010). Geochemistry of oceanic anoxic events: REVIEW. *Geochemistry, Geophysics, Geosystems*,. https://doi.org/10.1029/2009GC002788

Jin, H., Sonnenberg, S.A. (2013). Characterization for Source Rock Potential of the Bakken Shales in the Williston Basin, North Dakota and Montana. *Unconventional Resources Technology Conference, Denver, Colorado, 12-14 August 2013*, 117–126: https://doi.org/10.1190/urtec2013-013.

Kaltenbach, A. (2012). Uranium isotopic analysis of terrestrial and extraterrestrial samples. Ph.D. Dissertation, University of Otago, New Zealand.

Kendall, B., Wang, J., Zheng, W., Romaniello, S. J., Over, D. J., Bennett, Y., Xing, L., Kunert, A., Boyes, C., & Liu, J. (2020). Inverse correlation between the molybdenum and uranium isotope compositions of Upper Devonian black shales caused by changes in local depositional conditions rather than global ocean redox variations. *New Developments in Geochemical Proxies for Paleoceanographic Research*, *287*, 141–164. https://doi.org/10.1016/j.gca.2020.01.026

Kendall, B., Komiya, T., Lyons, T. W., Bates, S. M., Gordon, G. W., Romaniello, S. J., Jiang, G., Creaser, R. A., Xiao, S., McFadden, K., Sawaki, Y., Tahata, M., Shu, D., Han, J., Li, Y., Chu, X., & Anbar, A. D. (2015). Uranium and molybdenum isotope evidence for an episode of widespread ocean oxygenation during the late Ediacaran Period. *Geochimica et Cosmochimica Acta*, *156*, 173–193. https://doi.org/10.1016/j.gca.2015.02.025

Kulenguski, J., Gilleaudeau, G., Kaufman, A., Kipp, M, A., Tissot, F, L, H. Tyler J. Goepfert, T, J., Pitts, A, D., Pierantoni, P., Evans, M, N., Elrick, M., (In review). Temporally-offset uranium and carbon isotope excursions across Cretaceous OAE 2 indicate that the global spread of marine euxinia drove enhanced organic carbon burial. *Paleogeography, Paleoclimatology, Paleoecology*.

Laakso, T. A., & Schrag, D. P. (2019). A small marine biosphere in the Proterozoic. *Geobiology*, *17*(2), 161–171. https://doi.org/10.1111/gbi.12323

Lau, K.V., Macdonald, F.A., Maher, K., Payne, J.L. (2017). Uranium isotope evidence for temporary ocean oxygenation in the aftermath of the Sturtian Snowball Earth. *Earth and Planetary Science Letters*, *458*, 282–292: https://doi.org/10.1016/j.epsl.2016.10.043.

Lau, K. V., Hancock, L. G., Severmann, S., Kuzminov, A., Cole, D. B., Behl, R. J., Planavsky, N. J., Lyons, T. W. (2022). Variable local basin hydrography and productivity control the uranium isotope paleoredox proxy in anoxic black shales. *Geochimica et Cosmochimica Acta*, *317*, 433–456. https://doi.org/10.1016/j.gca.2021.10.011

Lu, X., Dahl, T.W., Zheng, W., Wang, S., & Kendall, B. (2020). Estimating ancient seawater isotope compositions and global ocean redox conditions by coupling the molybdenum and uranium isotope systems of euxinic organic-rich mudrocks. *Geochimica et Cosmochimica Acta*, *290*, 76–103: https://doi.org/10.1016/j.gca.2020.08.032.

McGhee, G. R. (1996). *The late Devonian mass extinction: the Frasnian/Famennian crisis*. Columbia University Press.

Montoya-Pino, C., Weyer, S., Anbar, A.D., Pross, J., Oschmann, W., van de Schootbrugge, B., Arz, H.W. (2010). Global enhancement of ocean anoxia during Oceanic Anoxic Event 2: A quantitative approach using U isotopes. *Geology*, *38*, 315–318: https://doi.org/10.1130/G30652.1.

Over, D.J. (2021). The Devonian-Carboniferous boundary in the United States. *Palaeobiodiversity and Palaeoenvironments, 101*, 529-540: https://doi.org/10.1007/s12549-020-00428-1.

Poulton, S. W., Fralick, P. W., & Canfield, D. E. (2010). Spatial variability in oceanic redox structure 1.8 billion years ago. *Nature Geoscience*, *3*(7), 486–490. https://doi.org/10.1038/ngeo889

Poulton, S.W., Canfield, D.E. (2011). Ferruginous conditions: A dominant feature of the ocean through Earth's history. *Elements*, *7*, 107–112: https://doi.org/10.2113/gselements.7.2.107.

Provo, L.J., Kepferle, R.C., Potter, P.E. (1977). Three Lick Bed: useful stratigraphic marker in Upper Devonian shale in eastern Kentucky and adjacent areas of Ohio, West Virginia and Tennessee. *United States Department of Energy Technical Report* MERC/CR-77-2.

Rabalais, N.N., W.-J. Cai, J. Carstensen, D.J. Conley, B. Fry, X. Hu, Z. Quiñones-Rivera, R. Rosenberg, C.P. Slomp, R.E. Turner, M. Voss, B. Wissel, and J. Zhang. 2014. Eutrophication-driven deoxygenation in the coastal ocean. Oceanography 27(1):172–183, http://dx.doi.org/10.5670/oceanog.2014.21.

Rabalais, N. N., & Turner, R. E. (2019). Gulf of Mexico Hypoxia: Past, Present, and Future. *Limnology and Oceanography Bulletin*, *28*(4), 117–124. https://doi.org/10.1002/lob.10351

Rolison, J.M., Stirling, C.H., Middag, R., Rijkenberg, M.J.A. (2017). Uranium stable isotope fractionation in the Black Sea: Modern calibration of the $^{238}U/^{235}U$ paleo-

redox proxy. *Geochimica et Cosmochimica Acta*, *203*, 69–88: https://doi.org/10.1016/j.gca.2016.12.014.

Romaniello, Stephen J; Herrmann, Achim D; Anbar, Ariel D (2013): Chemistry and isotope variations in primary precipitates for the Exuma Island region of the Bahamas. PANGAEA, https://doi.org/10.1594/PANGAEA.812000, In supplement to: Romaniello, SJ et al. (2013): Uranium concentrations and 238U/235U isotope ratios in modern carbonates from the Bahamas: Assessing a novel paleoredox proxy. Chemical Geology, 362, 305-316, https://doi.org/10.1016/j.chemgeo.2013.10.002

Sahoo, S.K., Gilleaudeau, G.J., Wilson, K., Hart, B., Barnes, B., Faison, T., Bowman, A., Larsen, T., Kaufman, A.J. (in press). Eustasy, euxinia, and the Late Devonian mass extinctions. *Nature*.

Sandberg, C.A., Mason, C.E., Work, D.M., 2002. Position of the Kinderhookian-Osagean boundary in northeastern Kentucky and southern Ohio. In: Geological Society of America Abstracts with Programs. A-88.

Schwark, L., Empt, P. (2006). Sterane biomarkers as indicators of palaeozoic algal evolution and extinction events. *Palaeogeography, Palaeoclimatology, Palaeoecology*, *240*, 225–236. https://doi.org/10.1016/j.palaeo.2006.03.050

Scott, C., Slack, J.F., Kelley, K.D. (2017). The hyper-enrichment of V and Zn in black shales of the Late Devonian-Early Mississippian Bakken Formation (USA). *Chemical Geology*, *452*, 24–33. https://doi.org/10.1016/j.chemgeo.2017.01.026

Stramma, L., Prince, E. D., Schmidtko, S., Luo, J., Hoolihan, J. P., Visbeck, M., Wallace, D. W. R., Brandt, P., & Körtzinger, A. (2012). Expansion of oxygen minimum zones may reduce available habitat for tropical pelagic fishes. *Nature Climate Change*, *2*(1), 33–37. https://doi.org/10.1038/nclimate1304

Stylo, M., Neubert, N., Wang, Y., Monga, N., Romaniello, S.J., Weyer, S., Bernier-Latmani, R. (2015). Uranium isotopes fingerprint biotic reduction. *Proceedings of the National Academy of Sciences*, *112*, 5619–5624: https://doi.org/10.1073/pnas.1421841112.

Tissot, F.L.H., Dauphas, N., 2015. Uranium isotopic compositions of the crust and ocean: age corrections, U budget and global extent of modern anoxia. *Geochimica et Cosmochimica Acta*, *167*, 113–143: https://doi.org/10.1016/j.gca.2015.06.034

White, D. A., Elrick, M., Romaniello, S., & Zhang, F. (2018). Global seawater redox trends during the Late Devonian mass extinction detected using U isotopes of marine limestones. *Earth and Planetary Science Letters*, *503*, 68–77. https://doi.org/10.1016/j.epsl.2018.09.020

Wignall, P. B., & Twitchett, R. J. (1996). Oceanic Anoxia and the End Permian Mass Extinction. *Science*, *272*(5265), 1155–1158. https://doi.org/10.1126/science.272.5265.1155

Zhang, F., Dahl, T. W., Lenton, T. M., Luo, G., Shen, S., Algeo, T. J., Planavsky, N., Liu, J., Cui, Y., Qie, W., Romaniello, S. J., & Anbar, A. D. (2020). Extensive marine anoxia associated with the Late Devonian Hangenberg Crisis. *Earth and Planetary Science Letters*, *533*, 115976. https://doi.org/10.1016/j.epsl.2019.115976

Zhang, F., Algeo, T. J., Romaniello, S. J., Cui, Y., Zhao, L., & Anbar, A. D. (2018) Congruent Permian-Triassic $\delta^{238}U$ records at Panthalassic and Tethyan sites: Confirmation of global-ocean anoxia and validation of the U-isotope paleoredox proxy. Geology 46, 327-330: https://doi.org/10.1130/G39695.1.

Zhang, F., Romaniello, S.J., Algeo, T.J., Lau, K.V., Clapham, M.E., Richoz, S., Herrmann, A.D., Smith, H., Horacek, M., Anbar, A.D. (2018). Multiple episodes of extensive marine anoxia linked to global warming and continental weathering following the latest Permian mass extinction. *Science Advances, 4*, e1602921: https://doi.org/10.1126/sciadv.1602921.

BIOGRAPHY

Before attending university, Randolph L Rutledge worked as a building designer. He received his Bachelor of Science in Earth Science from George Mason University in 2020. Mr. Rutledge began his studies in Earth Systems Science at George Mason University in 2020. After graduating, he plans to work for the federal government.